bioRxiv preprint doi: https://doi.org/10.1101/2022.01.20.477108; this version posted January 22, 2022. The copyright holder for this preprint (which was not certified by peer review) is the author/funder, who has granted bioRxiv a license to display the preprint in perpetuity. It is made available under aCC-BY-NC-ND 4.0 International license.

Triplet kinase-phosphatase targeting to overcome kinase inhibitor tolerance in brain tumor cells

Oxana V. Denisova[1], Joni Merisaari[1,2], Riikka Huhtaniemi[1], Xi Qiao[1], Laxman Yetukuri[1,3], Mikael Jumppanen[1], Amanpreet Kaur[1], Mirva Pääkkönen[1], Carina von Schantz-Fant[3], Michael Ohlmeyer[5,6], Krister Wennerberg[3,7], Otto Kauko[1], Raphael Koch[8], Tero Aittokallio[3,4,9], Mikko Taipale[10], Jukka Westermarck[1,2]*

Affiliations:

[1]Turku Bioscience Centre, University of Turku and Åbo Akademi University, Turku, Finland.

[2]Institute of Biomedicine, University of Turku, Turku, Finland

[3]Institute for Molecular Medicine Finland (FIMM), HiLIFE, University of Helsinki, Helsinki, Finland.

[4]Centre for Biostatistics and Epidemiology (OCBE), Faculty of Medicine, University of Oslo, Oslo, Norway.

[5]Icahn School of Medicine at the Mount Sinai, NY, USA.

[6]Atux Iskay LLC, Plainsboro, NJ, USA.

[7]Biotech Research & Innovation Centre, University of Copenhagen, Copenhagen, Denmark.

[8]University Medical Center Goettingen, Goettingen, Germany.

[9]Institute for Cancer Research, Department of Cancer Genetics, Oslo University Hospital, Oslo, Norway.

[10]Donnelly Centre, University of Toronto, Toronto, Canada.

*Corresponding author. Email: jukka.westermarck@bioscience.fi

bioRxiv preprint doi: https://doi.org/10.1101/2022.01.20.477108; this version posted January 22, 2022. The copyright holder for this preprint (which was not certified by peer review) is the author/funder, who has granted bioRxiv a license to display the preprint in perpetuity. It is made available under aCC-BY-NC-ND 4.0 International license.

Abstract

Kinase inhibitor tolerance of human glioblastoma is an unmet clinical challenge and a mechanistic enigma. Here, we demonstrate that glioblastoma cell tolerance to multi-kinase inhibition can be reverted by reactivation of Protein Phosphatase 2A (PP2A). To characterize kinase targets of clinical stage multi-kinase inhibitor UCN-01 synergizing with PP2A reactivation, we established a strategy, named Actionable Targets of Multi-kinase Inhibitors (AToMI). AToMI revealed AKT and mitochondrial pyruvate dehydrogenase kinases (PDK1-4) as the co-targets for UCN-01-elicited synthetic lethality with PP2A reactivation. Notably, heterogeneous glioblastoma and medulloblastoma models were tolerant to AKT and PDK1-4 inhibitor monotherapies, and their combinations, but were effectively inhibited by triplet therapy including pharmacological PP2A reactivation. Mechanistically, overcoming the kinase therapy tolerance by the triplet therapy could be explained by combinatorial effects on signaling rewiring between AKT and PDK1-4, decrease in mitochondrial oxidative phosphorylation, and BH3-only protein mediated apoptosis priming. The brain-penetrant triplet combination had a significant *in vivo* efficacy in intracranial glioblastoma and medulloblastoma models. Collectively, we present a generalizable approach to identify actionable co-targets of multi-kinase inhibitors and demonstrate that overcoming of the kinase inhibitor tolerance in brain tumor cells requires triplet targeting of AKT, PDK1-4, and PP2A.

bioRxiv preprint doi: https://doi.org/10.1101/2022.01.20.477108; this version posted January 22, 2022. The copyright holder for this preprint (which was not certified by peer review) is the author/funder, who has granted bioRxiv a license to display the preprint in perpetuity. It is made available under aCC-BY-NC-ND 4.0 International license.

Introduction

Even though kinase inhibitors have revolutionized cancer therapies, most tumors acquire resistance to kinase inhibitors (1,2). Especially in cancer types genetically associated with hyperactivation of kinase pathways, such as human glioblastoma, the clinically observed kinase inhibitor resistance is a mechanistic enigma (3-5). Acquired therapy resistance develops via two phases - first through adaptive development of a drug-tolerant cellular state, and later, stable resistance that often occurs through acquisition of genetic mutations (6). The emerging evidence strongly indicates that the drug-tolerance is initiated rapidly after drug exposure by non-mutational signaling rewiring, often mediated by phosphorylation dependent signaling pathways (7,8). Thereby, characterization of the phosphorylation-dependent signaling rewiring events, and kinases/phosphatases controlling the rewiring, is expected to provide novel approaches for targeting the tumor relapse at its roots (9).

In addition to the development of non-genetic therapy tolerance, lack of target specificity of kinase inhibitors is a major translational challenge (2). Recent studies demonstrate that only a few kinase inhibitors target selectively their intended kinase target, and that the therapeutic effects of many kinase inhibitors are mediated by inhibition of other than their assumed target kinase (10,11). The unselectivity of kinase inhibitors can be employed therapeutically in a case the multi-kinase inhibitor (MKI) (12). Of clinically approved MKIs, sunitinib has an FDA approval for the treatment of gastrointestinal stromal tumors and advanced renal cell carcinoma. Additionally, derivatives of the classical MKI staurosporine (STS), have reached the clinics. Midostaurin (PKC412) is approved for the treatment of FLT3-mutated acute myeloid

bioRxiv preprint doi: https://doi.org/10.1101/2022.01.20.477108; this version posted January 22, 2022. The copyright holder for this preprint (which was not certified by peer review) is the author/funder, who has granted bioRxiv a license to display the preprint in perpetuity. It is made available under aCC-BY-NC-ND 4.0 International license.

leukemia (12), whereas another STS derivative UCN-01 (7-hydroxystaurosporine), was tested in phase II clinical trials in metastatic melanoma and relapsed T-Cell Lymphomas (NCT00082017). However, it is well established that each of these clinically tested STS derivatives inhibit activities of up to 50 kinases with approximately similar efficiency (10,13,14). Further, the STS derivatives are compromised by their pharmacokinetic properties in a case of brain tumors as they do not cross the brain-blood barrier (BBB). Therefore, development of MKIs towards clinical use would benefit from a better understanding of the kinase targets mediating both the therapeutic and potential toxic effects in each disease application. On the other hand, systematic mapping of the kinase targets of each MKI might provide an opportunity for development of novel combination therapy approaches by combining more selective kinase inhibitors targeting only the preferred kinases with more preferential pharmacokinetic and pharmacodynamic profiles. However, generalizable strategies for analysis of actionable MKI targets are currently missing.

Glioblastoma (GB) is the most common primary brain tumor in adults associated with high degree of therapy resistance, tumor recurrence and mortality (5,15). Extensive genome-wide profiling studies have established receptor tyrosine kinase RTK/RAS/PI3K/AKT signaling as one of the core altered pathways contributing to GB disease progression (3,16). AKT pathway fuels aerobic glycolysis (17), and GB cells are notorious for employing aerobic glycolysis in energy production and survival (18,19). However, targeting of these deregulated signaling mechanisms have achieved dismal clinical response rates in GB (4,20,21). Furthermore, disappointing results have been obtained from combination of kinase inhibitors, including also the MKIs (21). In addition to challenges with drug delivery across the BBB with a number of kinase inhibitors, the failure of kinase targeted therapies in GB has been proposed to be

bioRxiv preprint doi: https://doi.org/10.1101/2022.01.20.477108; this version posted January 22, 2022. The copyright holder for this preprint (which was not certified by peer review) is the author/funder, who has granted bioRxiv a license to display the preprint in perpetuity. It is made available under aCC-BY-NC-ND 4.0 International license.

linked to the prevalence of kinase pathway-mediated rewiring mechanisms (21), and general apoptosis-resistance of glioblastoma stem-like cells (GSCs) (15).

Protein phosphatase-2A (PP2A) is a ubiquitous serine/threonine phosphatase. Some PP2A complexes act as tumor suppressors and their inhibition is required for human cell transformation (22,23). PP2A regulates several kinase pathways and drug resistance mechanisms, and PP2A inhibition in cancer cells has been shown to drive broad-range kinase inhibitor resistance (24). PP2A is frequently inactivated in GB by non-genetic mechanisms including overexpression of endogenous PP2A inhibitor proteins such as CIP2A, PME-1, SET and ARPP19 (25-27). We recently published proof-of-concept data that reversal of PME-1-mediated PP2A inhibition strongly sensitized GB cells to several kinase inhibitors, including clinically tested STS derivatives (28). However, the translational value of these results remained questionable as PME-1 was experimentally inhibited by siRNAs and STS molecules that do not cross the BBB. Recently, a series of BBB permeable small molecule activators of PP2A (SMAPs) have been developed (29). However, their effects on kinase inhibitor resistance in GB has not yet been addressed.

To leverage on the therapeutic potential of combination of MKIs with pharmacological PP2A reactivation for GB therapy (28), we established a generalizable multi-step strategy for characterization of Actionable Targets of Multi-kinase Inhibitors (AToMI). The results identify AKT and pyruvate dehydrogenase kinases (PDK1-4) as the targets of MKI UCN-01 in drug-induced synthetic lethality (SL)(30) in combination with PP2A reactivation. As a translationally relevant outcome, we demonstrate that triplet targeting of AKT, PDK and PP2A induced robust synergistic cell death across heterogeneous GB and medulloblastoma (MB) cell lines,

bioRxiv preprint doi: https://doi.org/10.1101/2022.01.20.477108; this version posted January 22, 2022. The copyright holder for this preprint (which was not certified by peer review) is the author/funder, who has granted bioRxiv a license to display the preprint in perpetuity. It is made available under aCC-BY-NC-ND 4.0 International license.

and resulted in significant *in vivo* therapeutic effects on intracranial tumor models of GB and MB. Mechanistically, we identify a role for PP2A in regulating mitochondrial metabolism and blunting therapy-induced signaling rewiring. Collectively, these results support the clinical observations that combinations of kinase inhibitors alone are not sufficient for overcoming kinase inhibitor therapy tolerance in brain cancers, but indicate that this can be achieved by further combination of kinase inhibitors with pharmacological reactivation of PP2A.

bioRxiv preprint doi: https://doi.org/10.1101/2022.01.20.477108; this version posted January 22, 2022. The copyright holder for this preprint (which was not certified by peer review) is the author/funder, who has granted bioRxiv a license to display the preprint in perpetuity. It is made available under aCC-BY-NC-ND 4.0 International license.

Results

Pharmacological reactivation of PP2A synergizes with a multi-kinase inhibitor UCN-01

Based on our previous data demonstrating that PME-1 effects in GB cell kinase inhibitor resistance are mediated by PP2A (28), we hypothesized that the recently developed PP2A reactivating compounds (SMAPs) (29) could provide a pharmacological approach to induce synthetic lethal (SL) drug interaction (30) with UCN-01 in GB cells (Fig. 1A). To test the hypothesis, we directly compared the synergy with UCN-01 and PP2A reactivation by either PME-1 depletion (31), or SMAP (NZ-8-061) treatment, on colony growth potential of T98G cells. As shown in Fig. 1B, PME-1 depletion (either by siRNA or by CRISPR/Cas9) or NZ-8-061 did not induce any significant growth defect but induced potent SL with UCN-01. The interaction between NZ-8-061 and UCN-01 was dose dependent and observed by using both compounds at concentrations that showed negligible monotherapy activity (Fig. 1C, D, S1A). Validating the particular potential of PP2A reactivation in kinase inhibitor sensitization (9), NZ-8-061 displayed synergistic activity with as low as 0.5-1 μM concentration, that is approximately 10-fold lower concentrations that has been previously shown to be required for monotherapy effects for the compound (25,32). To rule out that the synergy between NZ-8-061 and UCN-01 would be mediated by any potential non-selective targets of NZ-8-061, we used SMAPs DBK-794 and DBK-1154 derived from dibenzoapine tricyclic family, i.e. chemically different from NZ-8-061 (Fig. 1E). Both DBK-794 and DBK-1154 were originally used to demonstrate direct interaction between SMAPs and PP2A, and for mapping of their interaction region (32). Importantly, these chemically diverse PP2A reactivators all resulted

bioRxiv preprint doi: https://doi.org/10.1101/2022.01.20.477108; this version posted January 22, 2022. The copyright holder for this preprint (which was not certified by peer review) is the author/funder, who has granted bioRxiv a license to display the preprint in perpetuity. It is made available under aCC-BY-NC-ND 4.0 International license.

in identical drug interaction with UCN-01 (Fig. 1C, D, F, S1B). Together with identical synergy observed by genetic PP2A reactivation (Fig. 1B) (28), and induction of synergy with non-toxic low micromolar SMAP concentration (Fig. 1D), the use of SMAPs with different chemistry mitigate concerns that the SMAP effects would be related to potential non-selective effects reported using toxic (10-30 μM) concentrations of NZ-8-061 (a.k.a DT-061) (33). Induction of caspase 3/7 activity indicated that the mode of cell death by SMAP+UCN-01 combination was apoptosis (Fig. 1G), and the drug interaction was validated in multiple GB cell lines (Fig. 1H, S1B). Importantly, synergy between UCN-01 and NZ-8-061 was not observed in non-cancerous fibroblasts providing evidence for cancer selectivity of the drug interaction (Fig. S1D). The synergistic drug interaction in GB cells was also seen in hypoxic environment, which is a common resistance mechanism in GB (Fig. S1C).

bioRxiv preprint doi: https://doi.org/10.1101/2022.01.20.477108; this version posted January 22, 2022. The copyright holder for this preprint (which was not certified by peer review) is the author/funder, who has granted bioRxiv a license to display the preprint in perpetuity. It is made available under aCC-BY-NC-ND 4.0 International license.

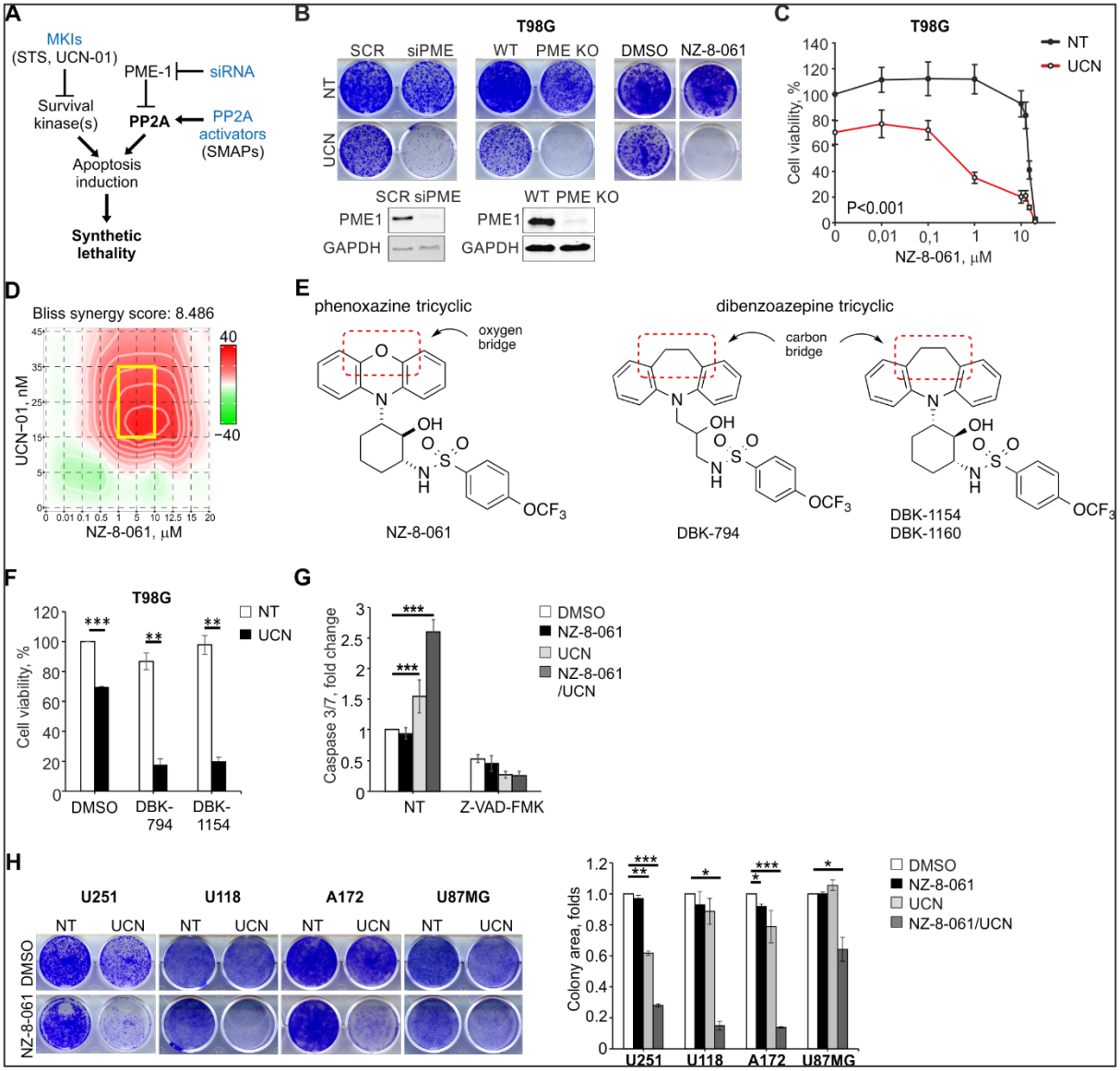

158

159 **Figure 1. PP2A reactivation and UCN-01 exert a synergistic effect in GB. A)** Schematic
160 illustrating PP2A reactivation predisposed to MKI-induced synthetic lethality in GB. **B)**
161 Representative images of colony formation assay in T98G cells under PME-1 siRNA-mediated
162 depletion, PME-1 KO or NZ-8-061 treatment. Cells were treated with 25 nM UCN-01 (UCN) or
163 left untreated (NT). Western blot analysis of PME-1 depletion or KO (lower panel). **C)** Viability
164 of T98G cells treated with increasing concentration of NZ-8-061 either alone or in
165 combination with 25 nM UCN-01 (UCN) for 72 h. Data as mean ± SD (n = 3 independent
166 experiments; ***P < 0.001, Student's *t*-test). **D)** Synergy plot showing the most synergistic
167 area (yellow box) between NZ-8-061 and UCN-01 in T98G cells. The Bliss synergy score is
168 calculated over the whole dose-response matrix. **E)** Structures of two different classes of
169 SMAPs exhibiting similar drug synergy with UCN-01. **F)** Viability of T98G cells treated SMAPs,
170 10 μM DBK-794 and 5 μM DBK-1154, alone or in combination with 25 nM UCN-01 for 72 h.
171 Data as mean ± SD (n = 2 independent experiments; **P < 0.01, ***P < 0.001, Student's t-
172 test). **G)** Caspase 3/7 activity in T98G cells treated with 8 μM NZ-8-061 alone or in combination

bioRxiv preprint doi: https://doi.org/10.1101/2022.01.20.477108; this version posted January 22, 2022. The copyright holder for this preprint (which was not certified by peer review) is the author/funder, who has granted bioRxiv a license to display the preprint in perpetuity. It is made available under aCC-BY-NC-ND 4.0 International license.

with 25 nM UCN-01 (UCN) for 24 h. The caspase inhibitor Z-VAD-FMK (20 µM) was added at the same time. Data as mean ± SD (n = 3 independent experiments; ***P < 0.001, Student's *t*-test). **H)** Representative images (left) and quantified data of colony formation assay (right) in U251, U118, A172 and U87 cells treated with 8 µM NZ-8-061 alone or in combination with UCN-01 (UCN; 200 nM, 25 nM, 50 nM and 500 nM, respectively). Data as mean ± SD (n = 2 independent experiments; *P < 0.05, **P < 0.01, ***P < 0.001, Student's *t*-test).

Strategy for characterization of Actionable Targets of Multi-kinase Inhibitors (AToMI)

Results above demonstrate strong synergistic activity between PP2A reactivation and multi-kinase inhibition by UCN-01. However, as UCN-01 targets approximately 50 different kinases at nanomolar concentrations (10,13), it remains unclear which one(s) of these kinases are involved in SL phenotype observed in combination with PP2A reactivation. To systematically map the UCN-01 co-target interactions, we devised a functional screening platform consisting of the following steps:

1) Chaperone interaction assay (34) to compare direct kinase binding between UCN-01 and other STS derivatives displaying differential synergism with PP2A reactivation in GB cells.

2) siRNA screening for synergistic interaction between PP2A reactivation and targeting of the individual kinase hits from the step 1.

3) Bioinformatics analysis of actionable kinase networks based on steps 1 and 2 for identification of selective small molecule inhibitors for the critical kinase nodes in the network.

4) Small molecule kinase inhibitor validation experiments.

As this strategy could be generally suitable for functional filtering of targets of MKIs, we hereby refer to the screening platform as characterization of Actionable Targets of Multi-kinase Inhibitors (AToMI) (Fig. 2). The individual technologies used in AToMI are

bioRxiv preprint doi: https://doi.org/10.1101/2022.01.20.477108; this version posted January 22, 2022. The copyright holder for this preprint (which was not certified by peer review) is the author/funder, who has granted bioRxiv a license to display the preprint in perpetuity. It is made available under aCC-BY-NC-ND 4.0 International license.

interchangeable with the most suitable technologies for any other application AToMI would be used for.

AToMI screening for UCN-01 target kinases involved in GB cell synthetic lethality in combination with PP2A reactivation

By using AToMI, we compared the kinase target profiles of STS analogues CEP-701, K252a, and UCN-01, previously shown to induce SL in PME-1 depleted T98G cells (28), as well as K252c and Rebeccamycin that did not induce SL when combined with PP2A reactivation (28). The differential synergistic activities of these STS derivatives in combination with NZ-8-061 was confirmed by colony growth assay (Fig. S2A). All five compounds were screened for their direct kinase protein binding against 300 kinases by chaperone interaction assay (34) (Fig. 2A, S2B, Table S1). This assay measures the interaction of kinases with their chaperone Cdc37 in the presence (or absence) of kinase inhibitors. Binding of the inhibitor to its target leads to thermodynamic stabilization of the target, which can be detected as weaker interaction between the kinase and Cdc37 (35).Using log2 -0.5-fold reduction in chaperone binding as a threshold for interaction, a total of 29 candidate kinases were identified to differentially interact with STS derivatives that synergized with PP2A (CEP-701, K252a, and UCN-01), but not with rebeccamycin or K252c (Table S2).

In the siRNA screening step of AToMI, the goal was to identify among the shared targets of CEP-701, K252a, and UCN-01, individual kinases whose co-inhibition resulted in a synergistic inhibition of cell viability with PP2A reactivation (Fig. 2B). The screen was conducted with a custom human kinase siRNA library, which had three non-overlapping siRNAs targeting each

bioRxiv preprint doi: https://doi.org/10.1101/2022.01.20.477108; this version posted January 22, 2022. The copyright holder for this preprint (which was not certified by peer review) is the author/funder, who has granted bioRxiv a license to display the preprint in perpetuity. It is made available under aCC-BY-NC-ND 4.0 International license.

kinases. In addition to 29 candidate kinases from the step 1, the siRNA library was extended to include 8 additional kinases frequently altered in GB (3,16) (Table S3). The siRNAs were reverse transfected to T98G cells, and cells were subsequently exposed to PP2A reactivation by NZ-8-061 treatment (Fig. 2B). In the validation screen, we included selected 25 kinases in combination with PME-1 siRNA to evaluate similarity in drug sensitization between chemical (NZ-8-061) and genetic (PME-1 siRNA) PP2A reactivation (Fig. 2B). The efficacy of PME-1 depletion by tree independent siRNAs was validated by western blotting from parallel samples (Fig. S2C). For each kinase siRNA, Gene Activity Ranking Profiles and synergy scores were computed as described in the methods section of siRNA screens. Notably, regardless of the marked differences in the targeting approaches, most of the kinases targeted in both screens were found to synergize both with NZ-8-061 treatment and PME-1 depletion (Fig. 2D), validating both the shared PP2A-induced mode of action, and the broad impact of PP2A activity in kinase inhibitor tolerance in GB.

STRING protein-protein interaction network analysis of the AToMI SL kinases from the step 2 revealed enrichment of RTK/RAF/MAPK (PDGFR, RAF1, BRAF, MAPK1) and PI3K/AKT/mTOR pathways (PIKCA, AKT1, AKT3), as well as mitochondrial pyruvate dehydrogenase kinase (PDK1 and PDK4) among the kinases, connected to PP2A B-subunits, previously shown to mediate SL between STS and PME-1 depletion (Fig. 2E) (28). As each of these kinase modules were represented also among the kinases that were shared between the NZ-8-061 and siPME-1 synergy targets, we proceeded to testing these GB signaling nodes by selective small-molecule inhibitors. Selectivity of the chosen small-molecule inhibitors was evaluated based recently published target selectivity databases, and for some compounds also by Chaperone interaction assay (Table S4) (10,14). To facilitate translation of the results, we also considered

bioRxiv preprint doi: https://doi.org/10.1101/2022.01.20.477108; this version posted January 22, 2022. The copyright holder for this preprint (which was not certified by peer review) is the author/funder, who has granted bioRxiv a license to display the preprint in perpetuity. It is made available under aCC-BY-NC-ND 4.0 International license.

247 oral bioavailability and BBB permeability of the compounds in drug selection. The selected 7
248 kinase inhibitors were screened for cell viability effects in T98G cells with two SMAPs, NZ-8-
249 061 and DBK-1154 (25). As a control, we used an inactive SMAP analog DBK-766, that binds
250 PP2A but is unable to reactivate it even at a concentration of 20 μM *in vitro* (32). The results
251 show that both NZ-8-061 and DBK-1154 sensitized T98G cells to MK-2206 and AKT1/2i (AKT
252 signaling) (36), and DCA (PDK1-4 inhibitor) (19,37) used at concentrations that engage their
253 aimed target kinase (Fig. S2D, E). Importantly, the inactive SMAP (DBK-766) did not synergize
254 with any of these kinase inhibitors (Fig. 2F). Further, RAF inhibitors (LY3009120 and
255 Vemurafenib), PI3K inhibitor (LY294002), or MINK1 inhibitor (mubritinib) did not display
256 significant combinatorial effect with PP2A reactivation (Fig. 2F). Importantly, another PDK
257 inhibitor, lipoic acid (37), recapitulated the synergy with SMAPs (Fig. S3A, B). In addition,
258 further validating the role of PP2A as a target for SMAPs in inducing the synergistic drug
259 interaction, PP2A reactivation by PME-1 inhibition also synergized with MK-2206 and DCA
260 treatments (Fig. S3C, D).
261
262 Collectively, these results demonstrate the usefulness of AToMI screening for identification
263 of individual actionable target kinases for MKIs. Regarding the UCN-01 target kinases involved
264 in SL with PP2A reactivation, AToMI screening resulted in selection of pharmacological
265 inhibitors of AKT pathway and mitochondrial PDK1-4 kinases for further functional validation.
266

bioRxiv preprint doi: https://doi.org/10.1101/2022.01.20.477108; this version posted January 22, 2022. The copyright holder for this preprint (which was not certified by peer review) is the author/funder, who has granted bioRxiv a license to display the preprint in perpetuity. It is made available under aCC-BY-NC-ND 4.0 International license.

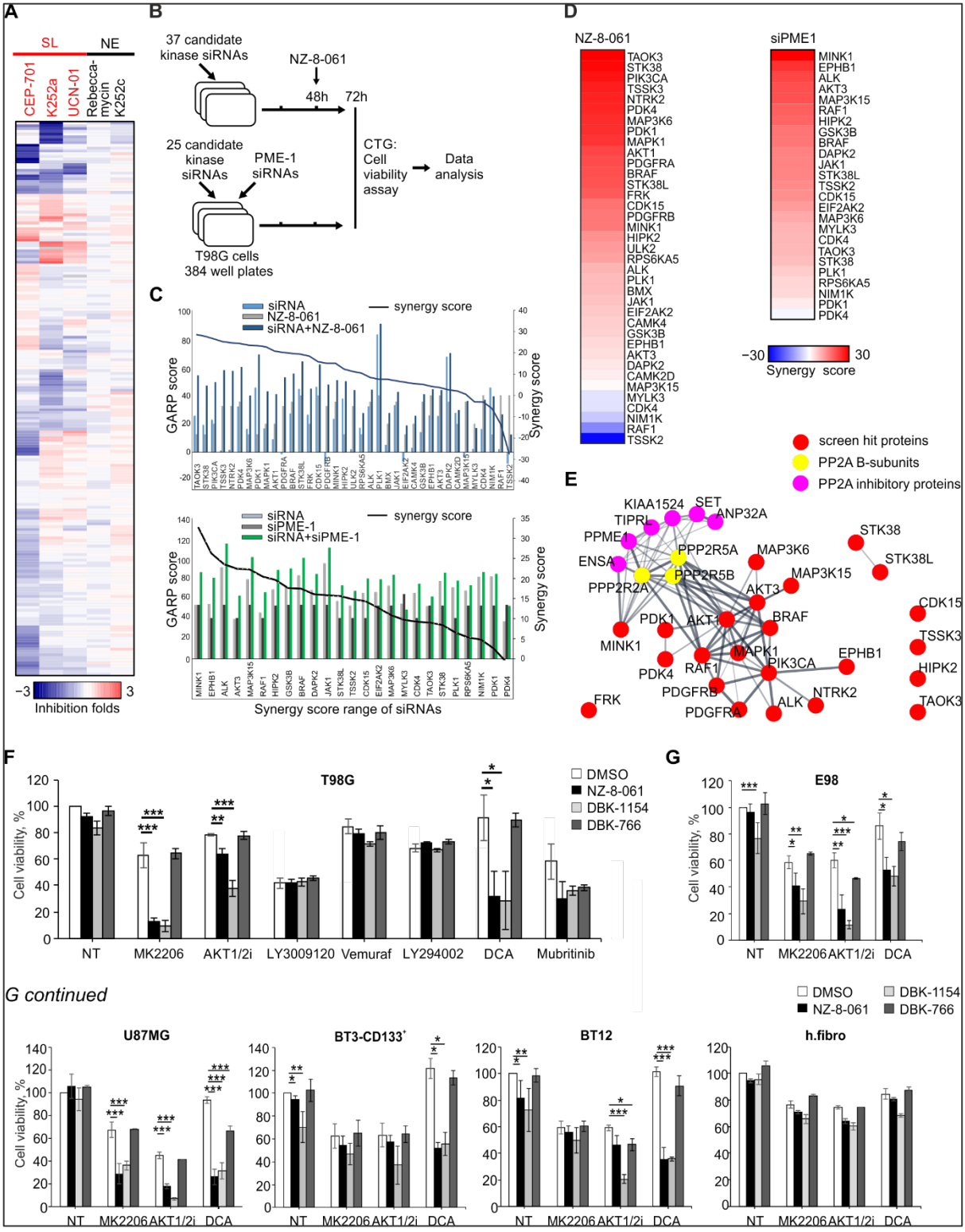

Figure 2. AToMI screening for UCN-01 target kinases involved in GB cell synthetic lethality in combination with PP2A reactivation. A) Heat map representation of interaction of STS derivatives, CEP-701, K252a, UCN-01, rebeccamycin and K252c, with 300 protein kinases by chaperone interaction assay. Color scale bar indicates log2 fold changes of kinase/Cdc37 interactions between inhibitor and DMSO treatments. SL - synthetic lethality, NE - no effect. **B)** Schematic illustrating of the performed kinase siRNA screens in T98G cells under NZ-8-061-

bioRxiv preprint doi: https://doi.org/10.1101/2022.01.20.477108; this version posted January 22, 2022. The copyright holder for this preprint (which was not certified by peer review) is the author/funder, who has granted bioRxiv a license to display the preprint in perpetuity. It is made available under aCC-BY-NC-ND 4.0 International license.

treatment or PME-1 depletion. **C)** GARP scores of siRNA screen in T98G cells under NZ-8-061- treatment or PME-1 depletion (left axis). Kinases were ordered according to synergy scores (right axis). **D)** Heat map representation of kinases involved in synthetic lethality in NZ-8-061-treated and PME-1-depleted T98G cells. Color bar indicates the synergy scores. **E)** STRING interactive mapping of screen kinase hits onto PP2A network. **F)** Viability of T98G cells and **G)** established GB, E98 and U87MG, and patient-derived GSCs, BT3-CD133^{+} and BT12, cell lines treated with the selected kinase inhibitors alone or in combination with 8 µM NZ-8-061, 6 µM DBK-1154 or 10 µM DBK-766 for 72 h. Human fibroblasts were used as a negative control cell line. Data as mean ± SD (n = 3 independent experiments). *P < 0.05, **P<0.01, ***P<0.001 by Student's *t*-test.

Triplet therapy induces cytotoxicity across heterogeneous GB cell lines

Cellular heterogeneity and high intrinsic therapy resistance of glioblastoma stem-like cells (GSCs) are major challenges related GB therapies (15). Therefore, we evaluated the synergy between AKT and PDK inhibitors with SMAPs across two additional established GB cell lines, and two patient-derived mesenchymal type GSC lines (BT-CD133^{+}, BT12) (25,38). Notably, western blot analysis revealed constitutive, but highly heterogeneous AKT and PDK1-4 activity across most of the brain tumor cell models used in this study (Fig. S4A). Consistently with high intrinsic kinase inhibitor resistance of GB cells (25,39), none of the kinase inhibitors as monotherapies, and used at doses that effectively inhibited their intended targets (Fig. S2D, E), did induce cytotoxic response (Fig. 2G). Further, albeit combination with SMAPs sensitized GB and GSC cells to a certain extent to AKT or PDK1-4 inhibition, the maximal co-inhibition of cell viability with double combinations was highly variable across the cell lines, and only some instances could be considered cytotoxic (Fig. 2G). Notably, the inactive SMAP analog DBK-766 did not synergize with any tested kinase inhibitor in any of the GB cell lines, and the human fibroblasts did not show any signs of synergy between kinase inhibition and SMAPs (Fig. 2G).

bioRxiv preprint doi: https://doi.org/10.1101/2022.01.20.477108; this version posted January 22, 2022. The copyright holder for this preprint (which was not certified by peer review) is the author/funder, who has granted bioRxiv a license to display the preprint in perpetuity. It is made available under aCC-BY-NC-ND 4.0 International license.

As these results indicate that single kinase inhibitors, even when combined with PP2A reactivation, cannot be used as a general strategy against heterogeneous GB cell populations, we decided to combine both AKT pathway and PDK1-4 inhibition together with PP2A reactivation as a triplet therapy. The rationale behind the triplet combination was that non-genetic signaling rewiring induced by single therapies (7,8) could be avoided by simultaneous targeting of two major kinase signaling nodes and by lowering the serine/threonine phosphorylation activity by PP2A. Even though both AKT inhibitors exhibited similar efficiency, we chose MK-2206 for the triplet therapy because of its frequent use in clinical trials (36). To assess long-term cytotoxic effects of the combinations, the triplet therapies were tested by using colony growth assays. Notably, fully supportive of therapy-induced therapy tolerance, all cell lines, except for T98G, were found to be resistant to cytotoxic effects of combined PDK (DCA) and AKT (MK-2206) inhibition (Fig. 3A, B). NZ-8-061 was found to potentiate effects of MK-2206 or DCA variably across the cell lines; most notably seen in E98 cells for MK-2206, and in BT3-CD133^{+} cells for DCA (Fig. 3A, B). However, the triplet therapy was the only drug combination that was found effectively eradicating all GB and GSC lines without notable effects on fibroblasts (Fig. 3A, B). This supports our hypothesis that triplet therapy is needed to tackle the heterogeneity of the therapy responses in GB.

Medulloblastoma (MB) is another brain tumor in which kinase inhibitors have been proven clinically ineffective (40). However, AKT, PDK and PP2A have all been implicated as potential targets for future MB therapies (40,41). Therefore, we studied whether the results above could be expanded from GB to MB. Reassuringly, when tested on two MB cell models, DAOY and D283-Med, representing SHH subtype and Group 3/4, respectively, we observed similar

bioRxiv preprint doi: https://doi.org/10.1101/2022.01.20.477108; this version posted January 22, 2022. The copyright holder for this preprint (which was not certified by peer review) is the author/funder, who has granted bioRxiv a license to display the preprint in perpetuity. It is made available under aCC-BY-NC-ND 4.0 International license.

synergistic drug interaction between MK-2206, DCA and SMAPs (NZ-8-061 and DBK-1160) as across the GB cell lines (Fig. 3C). In addition, in colony growth assay in DAOY cells, we confirmed that combination of AKT and PDK inhibition was not sufficient for potent cytotoxicity, whereas combination with SMAP DBK-1160 resulted in very potent SL phenotype (Fig. 3D).

To better understand the qualitative differences between GB cell responses to mono, double, and triplet therapies, we performed an Incucyte long-term confluency analysis in E98 cells treated with drugs twice for two weeks, with one week drug holiday in between (Fig. 3E). Although the E98 cells responded to all therapies during the first dosing period, the long-term data confirmed full resistance to each of the monotherapies. On the other hand, doublet combinations were found to be more efficient than monotherapies, but with all doublet combinations the effect was only cytostatic, as the cells were able to regain their proliferation after the drug wash-outs (Fig. 3E, see days 6-13 and 21-24). However, the triplet therapy treated cells were not able to escape the therapy during the follow-up and showed clear signs of cytotoxic response after initiation of the second dosing period (Fig. 3E, F).

Collectively, these results provide a strong validation to the AToMI screening results across genetically heterogeneous GB, GSC and MB cell lines. Importantly, the results clearly demonstrate that efficient shutdown of therapy tolerance across GB and MB cell lines requires combined inhibition of two kinases, and reactivation of PP2A phosphatase activity.

bioRxiv preprint doi: https://doi.org/10.1101/2022.01.20.477108; this version posted January 22, 2022. The copyright holder for this preprint (which was not certified by peer review) is the author/funder, who has granted bioRxiv a license to display the preprint in perpetuity. It is made available under aCC-BY-NC-ND 4.0 International license.

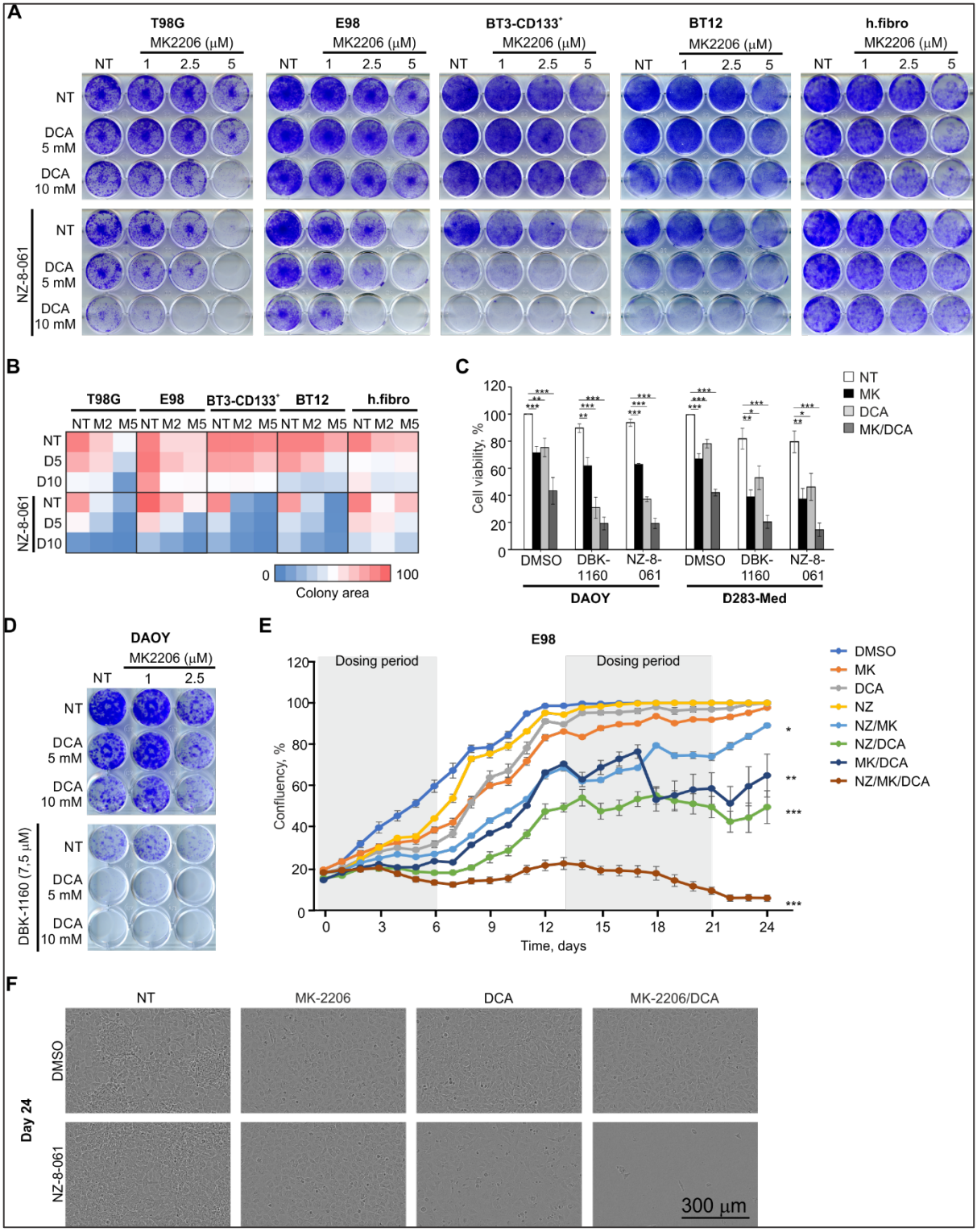

Figure 3. Triplet combination of NZ-8-061 with DCA and MK-2206 exert a synergistic cytotoxic effect in molecularly heterogeneous GB and MB cell lines. A) Representative images of colony growth assay in T98G, E98, BT3-CD133^{+}, BT12 and fibroblasts under triplet combination treatment as indicated. **B)** Heat map representation of quantified colony growth assay data in the indicated cell lines treated with MK-2206 (MK; 2.5 or 5 μM), DCA (D; 5 or 10 mM) or NZ-8-061 alone or in double or triplet combination. Human fibroblasts were used as

bioRxiv preprint doi: https://doi.org/10.1101/2022.01.20.477108; this version posted January 22, 2022. The copyright holder for this preprint (which was not certified by peer review) is the author/funder, who has granted bioRxiv a license to display the preprint in perpetuity. It is made available under aCC-BY-NC-ND 4.0 International license.

a negative control cell line (n=2 independent experiments). **C)** Cell viability in DAOY and D283-Med medulloblastoma cells treated with DMSO, 8 µM DBK-116 or 10 µM NZ-8-061 alone or in combination with 5 µM MK-2206 (MK), 20 mM DCA, or MK + DCA for 72 h. Data as mean ± SD (n = 3 independent experiments: *P<0.05, **P<0.01, ***P<0.001 by Student's t-test). **D)** Representative images of colony growth assay in DAOY cells under triplet combination as indicated. **E)** Proliferation of E98 cells treated with DMSO, 7 µM MK-2206 (MK), 20 mM DCA, 10 µM NZ-8-061 (NZ) alone or in double or triplet combinations. Data as mean ± SEM (n = 6 – 12 wells per condition). *P < 0.05, **P<0.01, ***P<0.001 by Kruskal-Wallis test to DMSO group. **F)** Representative pictures of E98 cells from (E) at day 24.

The triplet therapy blunts therapy-induced signaling rewiring and potentiates apoptosis induction

Fully consistent with the therapy-induced signaling rewiring hypothesis, we found that while MK-2206 efficiently inhibited the AKT S473 phosphorylation, it simultaneously enhanced, at least to certain extent in all cell lines, phosphorylation of a direct mitochondrial PDK1-4 target PDHE1α (Pyruvate Dehydrogenase E1 Subunit Alpha 1) (37) (Fig. 4A-C). In contrast, inhibition of PDK by DCA completely abolished phosphorylation of PDHE1α S300, but enhanced phosphorylation of AKT in T98G cells (Fig. 4A-C). However, combination of MK-2206 and DCA was able to shut-down phosphorylation of both proteins across all cell lines (Fig. 4A-C). NZ-8-061 treatment instead affected AKT and PDK signaling in very heterogeneous manner, depending on the kinase inhibitor combination, and the cell line. In other cell lines, except for T98G, DCA + NZ-8-061 combination inhibited AKT S473 phosphorylation, but instead resulted in less efficient PDHE1α S300 inhibition than with DCA alone (Fig. 4C). On the other hand, NZ-8-061 did rescue the compensatory PDHE1α S300 phosphorylation induced by MK-2206. NZ-8-061 also expectedly inhibited AKT phosphorylation across the cell lines, but very interestingly also synergized with DCA in AKT inhibition (Fig. 4A-C).

bioRxiv preprint doi: https://doi.org/10.1101/2022.01.20.477108; this version posted January 22, 2022. The copyright holder for this preprint (which was not certified by peer review) is the author/funder, who has granted bioRxiv a license to display the preprint in perpetuity. It is made available under aCC-BY-NC-ND 4.0 International license.

To correlate these findings to the apoptotic potential of the combination therapies, we examined PARP cleavage from the same cellular lysates. The data reveals that neither NZ-8-061 at doses that synergize in drug combinations, nor total shutdown of AKT and PDK signaling (MK-2206 + DCA) (Fig. 4B, C), was alone sufficient for maximal apoptosis induction in any of the studied GB cell lines (Fig. 4D). However, the highest apoptotic response was consistently seen across all cell lines upon the triplet therapy treatment (Fig. 4D). Lastly, DAOY MB cells displayed similar therapy-induced signaling rewiring between AKT and PDK pathways than in GB cells, but combination with DBK-1160 blunted the rewiring and resulted in potent apoptosis induction (Fig. S4B).

Collectively, these observations confirm prevalent therapy-induced signaling rewiring and heterogeneity in the combinatorial drug responses across the GB cells. Importantly, SMAP treatment was found to inhibit therapy-induced signaling rewiring, and thereby convert cytostatic kinase inhibitor responses to cytotoxic effects across GB cells. The results also strongly indicate that the discovered kinase pathway inhibition tolerance mechanism is shared between GB and MB.

bioRxiv preprint doi: https://doi.org/10.1101/2022.01.20.477108; this version posted January 22, 2022. The copyright holder for this preprint (which was not certified by peer review) is the author/funder, who has granted bioRxiv a license to display the preprint in perpetuity. It is made available under aCC-BY-NC-ND 4.0 International license.

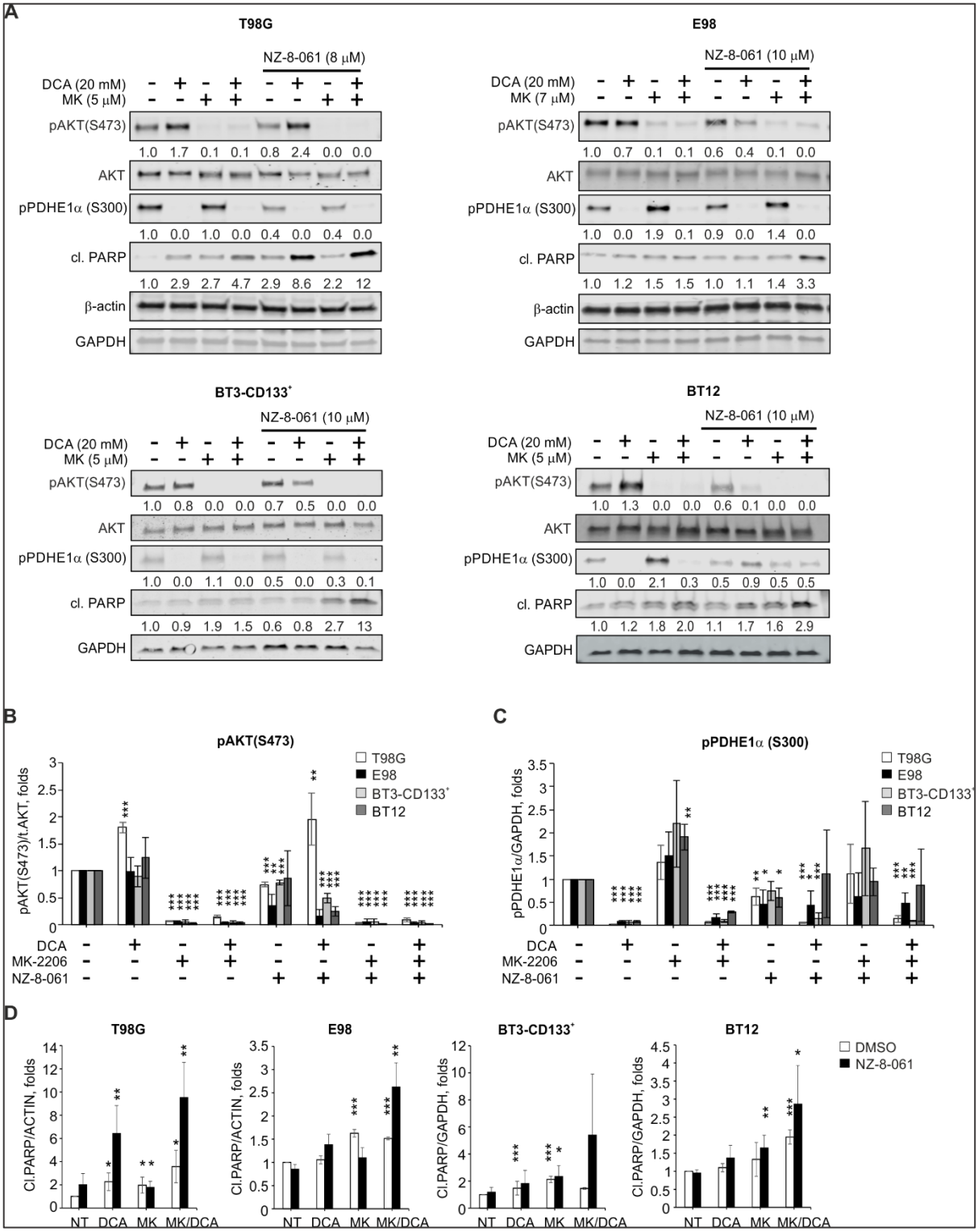

Figure 4. Inhibition of drug-induced signaling rewiring and apoptosis sensitization by the triplet therapy. A) Immunoblot assessment of phosphorylated AKT (S473), phosphorylated PDHE1α (S300), and cleaved PARP after treatment with MK-2206 (MK), DCA or NZ-8-061 alone or in double or triplet combination for 24 h in T98G, E98, BT3-CD133^{+} and BT12 cells. Normalized quantifications from (A) for **B)** phosphorylated AKT (S473) to total AKT, **C)**

bioRxiv preprint doi: https://doi.org/10.1101/2022.01.20.477108; this version posted January 22, 2022. The copyright holder for this preprint (which was not certified by peer review) is the author/funder, who has granted bioRxiv a license to display the preprint in perpetuity. It is made available under aCC-BY-NC-ND 4.0 International license.

phosphorylated PDHE1α to GAPDH, and **D)** cleaved PARP to β-actin. Data as mean ± SD (n = 3 independent experiments: *P < 0.05, **P<0.01, ***P<0.001 by Student's *t*-test).

Triplet therapy inhibits mitochondrial OXPHOS and primes to BH3 protein-mediated apoptosis

The above results revealed an interesting crosstalk between cytoplasmic AKT and mitochondrial PDK1-4 signaling. PP2A inhibition by CIP2A was recently implicated in regulation of mitochondrial oxidative phosphorylation (OXPHOS) (42). Specifically, PP2A reactivation by CIP2A inhibition resulted in inhibition of maximal mitochondrial respiration, decrease in spare oxidative capacity, and decrease in ATP production (42). To analyze whether apoptosis-sensitizing effect of pharmacological PP2A reactivation observed above would be associated with defects in OXPHOS, the T98G cells were exposed to either MK-2206 or DCA alone, or in combination with NZ-8-061, and analyzed by Seahorse Real-Time XF Analyzer (see Materials and Methods for details). As excepted, DCA alone increased ATP production, as it reactivates the OXPHOS in the mitochondria (Fig. 5A, B) (37,43). On the contrary, MK-2206 reduced ATP production and mitochondrial-linked respiration (Fig. 5B). Interestingly, NZ-8-061 used at SL inducing non-toxic concentration had a broad-spectrum effect on mitochondrial metabolism. Especially interesting drug interaction was inhibition of DCA-induced OXPHOS (Basal, Maximal, and Spare), indicating that PP2A reactivation can prevent compensatory mitochondrial survival mechanism. NZ-8-061 alone, and in combination with MK-2206, also profoundly increased proton leak indicating for mitochondrial membrane damage (Fig. 5A, B).

bioRxiv preprint doi: https://doi.org/10.1101/2022.01.20.477108; this version posted January 22, 2022. The copyright holder for this preprint (which was not certified by peer review) is the author/funder, who has granted bioRxiv a license to display the preprint in perpetuity. It is made available under aCC-BY-NC-ND 4.0 International license.

Based on recently published results, the inner mitochondrial impairment on OXPHOS, and increased proton leakage, potently interact with BH3-only protein mediated apoptosis regulation in the outer mitochondrial membrane (44). Therefore, we also characterized the impact of drug combinations on mitochondrial cytochrome *c* release. In line with other findings (Fig. 3C and 4D), we observed limited cytochrome *c* release by single drug treatment with NZ-8-061, DCA or MK-2206 or with double NZ-8-061 + DCA or NZ-8-061 + MK-2206 combinations (Fig. 5C). In contrast, the triplet therapy induced strong cytochrome *c* release (Fig. 5C). As cytochrome *c* release is controlled by BH3-only proteins on the outer mitochondrial membrane (45), we eventually wanted to clarify the functional interaction between cytoplasmic AKT, and mitochondrial PDK1-4 kinases on regulation of mitochondrial apoptosis by dynamic BH3 profiling. BH3 profiling uses a library of synthetic peptides to elucidate mechanisms by which cell evade apoptosis and dissect the functional relevance of each BCL2 family member (46,47). BH3 profiling revealed a limited impact on apoptotic priming by PDK1-4 inhibition, but a marked increase in the cells' susceptibility towards BIM, HRK, and MS1 mediated cytochrome *c* release when AKT was inhibited (Fig. 5D). Notably, there was a marked enhancement and broadening of BH3-mediated apoptosis priming when AKT and PDK1-4 were co-inhibited, providing an additional explanation for their synergistic pro-apoptotic effect (Fig. 5E). Results related to the impact of triplet therapy on BH3 profiling were inconclusive presumably due to high apoptotic activity (data not shown).

Collectively, these data identify multiple mitochondrial converge points between AKT, PDK1-4 and PP2A signaling. They also reveal the mechanistic basis for the high apoptotic activity of the triplet therapy due to NZ-8-061-elicited inhibition of the compensatory OXPHOS, and inner mitochondrial membrane proton leakage, combined with synergism between MK-2206

bioRxiv preprint doi: https://doi.org/10.1101/2022.01.20.477108; this version posted January 22, 2022. The copyright holder for this preprint (which was not certified by peer review) is the author/funder, who has granted bioRxiv a license to display the preprint in perpetuity. It is made available under aCC-BY-NC-ND 4.0 International license.

451 and DCA on BH3 priming. Notably, the synergistic interaction between inner mitochondrial
452 dysfunction (OXPHOS and proton leakage) and BH3 priming in apoptosis induction is
453 consistent with recent findings in other cancer types (44).

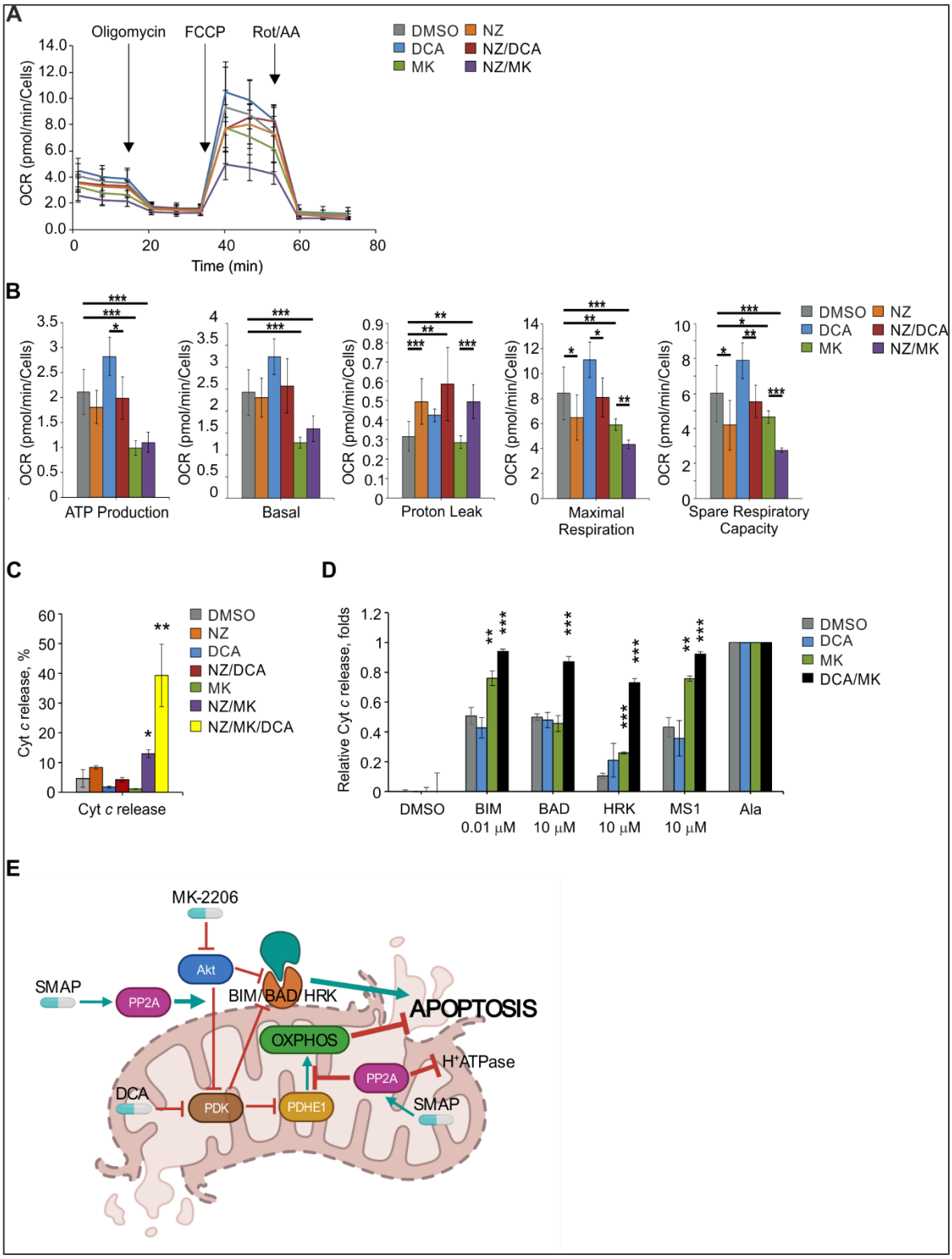

454

bioRxiv preprint doi: https://doi.org/10.1101/2022.01.20.477108; this version posted January 22, 2022. The copyright holder for this preprint (which was not certified by peer review) is the author/funder, who has granted bioRxiv a license to display the preprint in perpetuity. It is made available under aCC-BY-NC-ND 4.0 International license.

Fig. 5. Triplet therapy inhibits mitochondrial OXPHOS and primes to BH3 protein-mediated apoptosis A) Mitochondrial stress test Seahorse profile in T98G cells treated with 10 mM DCA or 7 µM MK-2206 (MK) alone or in combination with 10 µM NZ-8-061 (NZ) for 24 h. **B)** Mitochondrial parameters from (A). Data as mean ± SD (n = 3 independent experiments; *P < 0.05, **P<0.01, ***P<0.001 by Student's t-test). **C)** Cytochrome c release from T98G cells treated with 5 µM MK-2206 (MK), 20 mM DCA or 8 µM NZ-8-061 (NZ) alone or in double or triplet combination for 24 h. Data as mean ± SD (n = 3, *P < 0.05, **P<0.01, ***P<0.001 by Student's *t*-test). **D)** Priming of T98G cells to apoptosis induction by indicated BH3 peptides. 5 µM MK-2206 (MK), 20 mM DCA were used alone or combination for 24 h. Data as mean ± SD (n = 3, *P < 0.05, **P<0.01, ***P<0.001 by Student's *t*-test) **E)** Schematic illustration of mitochondrial mechanisms for triplet therapy-induced apoptosis based on Fig. 4 and 5. Inhibition of PDK1-4 induces compensatory OXPHOS but this is blunted by SMAP treatment which additionally induces mitochondrial membrane proton leakage. PDK1-4 and AKT inhibition synergizes on BH3-meidated apoptosis priming and SMAP treatment inhibits signaling rewiring between the kinases. Whereas in response to doublet drug combinations cells can induce some compensatory survival mechanism, these are simultaneously inhibited in triplet therapy treated cells resulting in terminal apoptosis induction.

Validation of therapeutic potential of the triplet therapy in orthotopic GB and medulloblastoma models

In vivo relevance of the results was investigated in subcutaneous and intracranial models using both E98 GB cells and DAOY MB cells. First, we wanted to provide *in vivo* validation to AToMI screening results that the SL effects of SMAPs with UCN-01 can be recapitulated by combination of AKT and PDK inhibition. As UCN-01 does not cross the BBB, these experiments were performed using subcutaneous xenografts, and instead of NZ-8-061, we used DBK-1160 as a SMAP due to its better pharmacokinetic profile based on our previous studies (data not shown). Fully validating the results from AToMI approach, the orally dosed triplet therapy (DBK-1160 + MK-2206 + DCA) was equally efficient, or even superior to combination of DBK-1160 and UCN-01 (Fig. 6A, B). The robust *in vivo* antitumor effect of the triplet therapy in DAOY model was readily seen also when comparing the sizes of the excised tumors (Fig. 6C).

bioRxiv preprint doi: https://doi.org/10.1101/2022.01.20.477108; this version posted January 22, 2022. The copyright holder for this preprint (which was not certified by peer review) is the author/funder, who has granted bioRxiv a license to display the preprint in perpetuity. It is made available under aCC-BY-NC-ND 4.0 International license.

To molecularly profile the triplet therapy effect in the treated tumors, the vehicle and the triplet therapy treated tumors (n=5 for both) were subjected to mass spectrometry phosphoproteomics analysis using TMT-labeling. Upon filtering the data for those phosphopeptides there were quantifiable from at least three tumors per group, and with FDR of 5% for significance of the difference in phosphopeptide expression between the groups (Table S5), the Reactome pathway analysis validated the impact triplet therapy on both apoptosis and cell cycle, but on the other hand revealed a very strong enrichment of targets involved in “Signaling by Rho GTPases” (Fig. 6D, S5, Table S6). Furthermore, fully consistent with our model that efficient therapy response in brain tumors requires wide-spread kinase inhibition, we found inhibition of phosphorylation of several kinases from the triplet therapy treated tumors (Fig. 6E, Table S5). Notably, among those were inhibition of the phosphorylation of the activation loop of AKT1, 2 and 3, which together with enrichment of mTOR signaling based on phosphopeptide data (Fig. 6E, Table S5), perfectly supports our mechanistic data demonstrating importance of the shutdown of rewiring to AKT signaling (Fig. 4). Inhibition of AKT signaling was evident also based on kinase target motif enrichment analysis where canonical AKT target motifs (R-x-R-x-x-S/T and R-x-x-S/T) were clearly enriched in the phosphopeptides downregulated by the triplet therapy (Fig. 6I). Beside AKT, among the dephosphorylated kinases were also the pro-survival downstream targets of ERK MAPK, RSK1 and 3, as well as transcriptional elongation promoting kinase CDK9, that is essential for brain tumor-initiating cells (48), and a synergistic drug target with SMAPs (49). Additional exploration of the data by NetworKIN analysis, revealed enrichment of CDK1 and CDK5 targets (Fig. S6A). CDK5 is a known neuronal kinase activated in GB and MB, and CDK1 regulation links very well to enrichment of cell cycle/mitosis based on phoshopeptide data (Fig. 6D).

bioRxiv preprint doi: https://doi.org/10.1101/2022.01.20.477108; this version posted January 22, 2022. The copyright holder for this preprint (which was not certified by peer review) is the author/funder, who has granted bioRxiv a license to display the preprint in perpetuity. It is made available under aCC-BY-NC-ND 4.0 International license.

510 Interestingly, but consistent with the therapy-induced non-genetic signaling rewiring, we also
511 identified a number phosphopeptides upregulated in the triplet therapy treated tumors (Fig.
512 6F; upper right corner and Table S5). Related to kinase signaling, we noticed that several
513 kinases involved in the pro-apoptotic JNK and p38 MAPK signaling were hyperphosphorylated
514 in the treated tumors (Fig. S6B), and both JNK1 and JNK2 were among the top enriched kinase
515 target motifs based on NetworKIN analysis (Fig. S6A). As both JNK and p38 are involved
516 apoptosis regulation by BH3 proteins (50), these data provide a plausible link between the
517 proposed mechanism for triplet therapy induced brain tumor cell killing (Fig. 5E), and the
518 observed in vivo therapeutic effects (Fig.6F).
519
520 Finally, in intracranial model the triplet therapy was tested on luciferase-expressing E98 cells
521 that carry characteristics of GSCs and has very infiltrative growth pattern *in vivo* (25). In
522 addition to these faithful human GB characteristics, E98 cells displayed indistinguishable
523 triplet therapy response as compared to patient derived GSC cell lines *in vitro* (Fig. 3).
524 Importantly, we observed significant inhibition of tumor growth by orally dosed triplet
525 therapy initiated upon appearance of detectable tumors at day 10 (Fig. 6G). For DAOY cells,
526 we relied on mouse survival as the end-point measurement of the therapy effect, since no
527 tumor growth visualization approaches were available for these tumors. Remarkably, more
528 than 50% of the vehicle treated mice died during the therapy, whereas in the triplet therapy
529 group only one mouse had to be sacrificed due to neurological symptoms (Fig. 6H). Following
530 cessation of therapy after 30 days, due to local regulations, we observed a significant increase
531 in mouse survival in the triplet therapy group, associated with 26-day prolongation of the
532 median probability of survival (Fig 6H). No obvious toxicities were observed during triplet
533 therapy treatment periods in either subcutaneous or intracranial models (Fig. S7). However,

bioRxiv preprint doi: https://doi.org/10.1101/2022.01.20.477108; this version posted January 22, 2022. The copyright holder for this preprint (which was not certified by peer review) is the author/funder, who has granted bioRxiv a license to display the preprint in perpetuity. It is made available under aCC-BY-NC-ND 4.0 International license.

534 as expected, the SMAP treatment resulted in reversible increase in liver weight, as has been

535 reported earlier (32).

536

537 Collectively, the subcutaneous tumor results provide *in vivo* validation that AKT and PDK are

538 the target kinases for the SL-inducing effect of UCN-01 in PP2A reactivated brain tumor cells.

539 The results further validate the translational relevance of the results in independent

540 orthotopic tumor models of common human brain tumors.

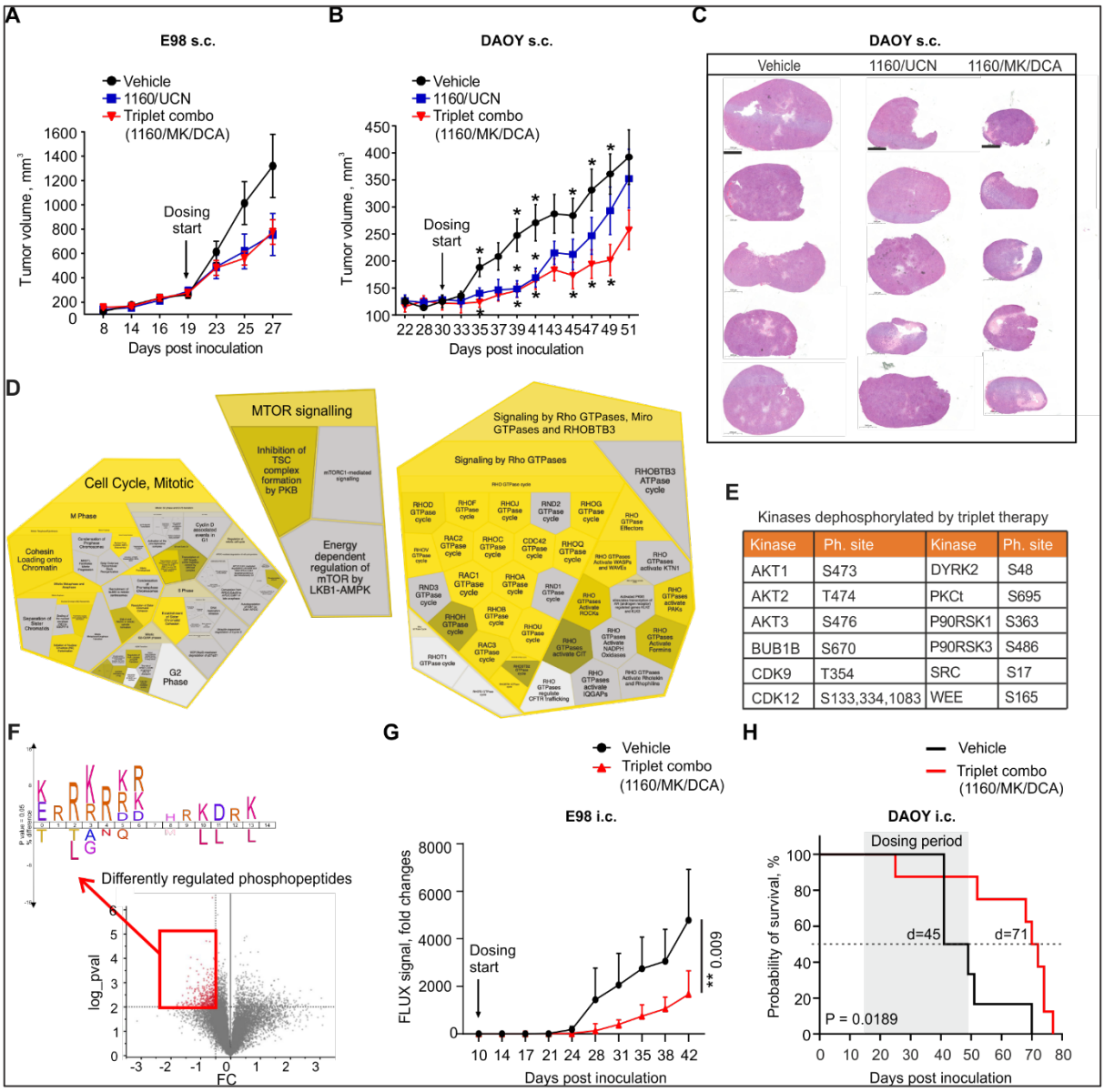

Kinase	Ph. site	Kinase	Ph. site
AKT1	S473	DYRK2	S48
AKT2	T474	PKCt	S695
AKT3	S476	P90RSK1	S363
BUB1B	S670	P90RSK3	S486
CDK9	T354	SRC	S17
CDK12	S133,334,1083	WEE	S165

541

bioRxiv preprint doi: https://doi.org/10.1101/2022.01.20.477108; this version posted January 22, 2022. The copyright holder for this preprint (which was not certified by peer review) is the author/funder, who has granted bioRxiv a license to display the preprint in perpetuity. It is made available under aCC-BY-NC-ND 4.0 International license.

Fig. 6. Validation triplet combination therapy in vivo. A-B) Quantification of tumor volume from E98 (A) and DAOY (B) s.c. tumors in mice treated with DBK-1160 (1160; 100 mg/kg twice a day) and UCN-01 (UCN; 3 mg/kg once a day) or MK-2206 (MK; 100 mg/kg every second day) and DCA (100 mg/kg twice a day), or vehicle control. Each group had n=8 mice in E98, n=10 mice in DAOY experiments. Mean ± SD. *P < 0.05 by two-way ANOVA test. **C)** Representative images from H&E staining of DAOY s.c. tumors from (B, n=5). Scale bar, 1000 µm. **D)** Reactome processes based on significantly (p< 0.05) regulated phosphopeptides from triplet therapy treated DAOY xenografts in (B). **E)** Kinases dephosphorylated by triplet therapy in DAOY xenografts from (B). **F)** Volcano plot showing differentially regulated phosphopeptides from (B). Icelogo kinase motif enrichment analysis from the dephosphorylated peptides (in red) (p≤0.01, log2FC ≤ -0.5) revealed enrichment of canonical AKT sites (R-x-R-x-x-S/T and R-x-x-S/T). **G)** Bioluminescence follow up of an orthotopic E98 glioblastoma tumor comparing the vehicle or triplet combination therapies (DBK-1160 (100 mg/kg twice a day) + MK-2206 (100 mg/kg every second day) + DCA (100 mg/kg twice a day)). Mean ± SEM. (n=10 mice per group). **P < 0.01 by Student's t-test. **H)** Kaplan–Meier survival analysis of xenograft orthotopic DAOY model treated with triplet combination (DBK-1160 (100 mg/kg twice a day) + MK-2206 (100 mg/kg every second day) + DCA (100 mg/kg twice a day)). Vehicle n=6, Triplet combo n=8 mice per group. Mantel-Cox test. * P <0.05.

bioRxiv preprint doi: https://doi.org/10.1101/2022.01.20.477108; this version posted January 22, 2022. The copyright holder for this preprint (which was not certified by peer review) is the author/funder, who has granted bioRxiv a license to display the preprint in perpetuity. It is made available under aCC-BY-NC-ND 4.0 International license.

Discussion

Kinase inhibitor resistance of brain tumors is a notable unmet clinical challenge (4,21,40). Considering that hyper activated kinase signaling is one of the hallmarks of GB (3,15), clinical resistance of GB to kinase inhibitors constitutes a mechanistic enigma. One of the potential reasons for ineffectiveness of kinase inhibitors in inhibition of oncogenic phosphorylation in GB is that phosphatases have not been taken into the account when designing the GB therapy strategies. There is a very strong theoretical basis for synergistic activities of simultaneous kinase inhibition and phosphatase activation in phosphorylation-dependent cancers (9,29), but the therapeutic impact of such combinatorial approach in overcoming therapy tolerance in brain cancers has been thus far unclear. Our results, using a panel of heterogeneous GB and MB cell lines, provide convincing proof-of-principle evidence that overcoming kinase inhibitor tolerance in brain cancers requires simultaneous multi-kinase inhibition and PP2A phosphatase activation.

MKIs provide an attractive approach to simultaneously inhibit several oncogenic kinases, and some MKIs (e.g., Sunitinib, PKC412), are clinically used as cancer therapies (12). However, similar to more selective kinase inhibitors, all tested MKIs have thus far failed in GB clinical trials (4). STS derivatives targeting more than 50 kinases (13) could provide a wide enough polypharmacological kinase inhibitor spectrum to target GB driver mechanisms, even in the case of heterogeneous GB cell populations. However, use of STSs as GB therapeutics is compromised by their inability to cross BBB. To overcome these limitations, and to better understand GB relevant STS target kinases, we developed the AToMI approach. As a result,

bioRxiv preprint doi: https://doi.org/10.1101/2022.01.20.477108; this version posted January 22, 2022. The copyright holder for this preprint (which was not certified by peer review) is the author/funder, who has granted bioRxiv a license to display the preprint in perpetuity. It is made available under aCC-BY-NC-ND 4.0 International license.

583 we found 29 kinases which selectively bound to STS derivatives and synergized with PP2A
584 reactivation by either PME-1 inhibition or by SMAPs (Fig. 2A, S2B). Notably, the kinases which
585 synergized with PP2A reactivation represent the commonly hyper activated pathways in GB.
586 For example, AKT pathway is one of the most dysregulated pathways in GB, and it was well
587 presented in the siRNA screen as depletion of AKT1, AKT3 and PIK3CA all synergized with PP2A
588 reactivation (Fig 2C, D). Another strongly GB associated signaling mechanism was
589 mitochondrial glycolysis, as depletion of both PDK1 and PDK4 synergized with PP2A
590 reactivation (Fig 2C, D). PDK kinases are key regulators of metabolic shift from OXPHOS to
591 glycolysis, which promotes GB tumor growth and resistance to therapies (18,19). However,
592 similar to other kinase inhibitor therapies, also AKT and PDK1-4 targeting monotherapies have
593 failed to demonstrate significant survival effects in clinical trials for GB (37,51-53). Our
594 subsequent kinase inhibitor combination experiments, using inhibitors at doses that inhibit
595 their target kinases, validate the ineffectiveness of AKT and PDK1-4 targeting in eradicating
596 heterogeneous GB cell lines (Fig. 3A, B). While all double therapies tested here, involving
597 either two kinase inhibitors, or one kinase inhibitor combined with SMAP, resulted at best in
598 cytostatic effect, the triplet therapy induced cytotoxic response considered as clinically
599 efficacious (Fig. 3A, B). Collectively, these results validate the usefulness of AToMI approach
600 for future studies aiming to characterize actionable targets of MKIs in different indications.
601 The AToMI approach also facilitated the identification of BBB permeable kinase inhibitors
602 with similar biological activity than UCN-01. This allowed validation of all main conclusions of
603 this study *in vivo* in two brain cancer orthotopic models displaying both significant therapeutic
604 effect with the triplet therapy.
605

bioRxiv preprint doi: https://doi.org/10.1101/2022.01.20.477108; this version posted January 22, 2022. The copyright holder for this preprint (which was not certified by peer review) is the author/funder, who has granted bioRxiv a license to display the preprint in perpetuity. It is made available under aCC-BY-NC-ND 4.0 International license.

606 Phosphorylation-dependent signaling rewiring after therapy is a prevalent mechanism for
607 cancer cells to escape apoptotic cell killing (7,8). Consistent with this model, we found that
608 AKT inhibition by MK-2206 induced phosphorylation of the PDK1-4 target PDHE1α in GB and
609 MB cells (Fig. 4A-B, S4B). We also validate *in vivo* inhibition of signaling rewiring to AKT and
610 mTOR in triplet therapy treated MB tumors (Fig. 6D-F). Notably, the therapy-induced signaling
611 rewiring between AKT and PDK pathways was abolished when MK-2206 and DCA were
612 combined, yet it failed to induce efficient apoptosis across the GB and MB cell lines, except
613 for the most sensitive T98G cells (Fig. 3A-C, 4D). PP2A reactivation by SMAPs altered brain
614 tumor cells response to MK-2206 and DCA in multiple ways. Consistent with the established
615 role of PP2A as an AKT phosphatase (23), SMAPs reduced the basal AKT S473 phosphorylation,
616 but surprisingly also strongly synergized with DCA in AKT dephosphorylation in most of the
617 studied cell lines. In addition, PP2A reactivation inhibited signaling rewiring by restraining MK-
618 2206-induced PDHE1α S300 phosphorylation. Interaction between PP2A and PDK was also
619 observed at the level of mitochondrial metabolism. NZ-8-061 decreased basal, spare, and
620 maximal respiratory capacity, and blunted the DCA-induced increase in OXPHOS. Importantly,
621 previous data indicate OXPHOS induction in response to inhibition of glycolysis (such as is
622 seen in DCA-treated cells) as a rescue mechanism protecting cells from apoptosis (54).
623 Furthermore, NZ-8-061 caused mitochondrial inner membrane proton leak which decreases
624 mitochondrial membrane potential leading to higher probability of apoptosis (55).
625
626 Collectively, our data identity a strategy for killing of heterogeneous brain tumor cells based
627 on MKI combined with PP2A reactivation. Specifically, through AToMI approach we identify
628 AKT and PDK1-4 as the critical UCN-01 target kinases involved in synthetic lethality when
629 combined with either genetic or pharmacological PP2A reactivation. Notably, our results are

bioRxiv preprint doi: https://doi.org/10.1101/2022.01.20.477108; this version posted January 22, 2022. The copyright holder for this preprint (which was not certified by peer review) is the author/funder, who has granted bioRxiv a license to display the preprint in perpetuity. It is made available under aCC-BY-NC-ND 4.0 International license.

630 relevant across heterogeneous GB and MB models including patient-derived GSCs. Further,
631 PP2A activation was found to sensitize GB cells against majority of the kinases tested by the
632 AToMI approach (Fig. 2D), hence providing a rich source for kinase inhibitor combinations to
633 be validated in the future studies. Combined with the previously demonstrated role for PP2A
634 in impacting lung cancer cell responses to over dozens of kinase inhibitors (24), our results
635 indicate that the uniform kinase inhibitor resistance observed in GB and MB clinical trials (4),
636 could be to significant extent contributed to non-genetic PP2A inhibition by its inhibitor
637 proteins (25,28,40,56). In this regard, diagnostic definition of PP2A inhibitor protein status
638 would greatly simplify biomarker-based analysis of PP2A activity in brain tumors because it
639 sidesteps the need for analyzing all the possibly relevant PP2A subunits. Specifically, the
640 current results encourage future brain tumor clinical trials with combinations of clinically
641 tested AKT and PDK1-4 inhibitors (20,51,53) in a significant proportion of brain cancer
642 patients with low tumor expression of PME-1 (28). Finally, our results strongly indicate that
643 rapidly developing PP2A reactivation therapies (29) will constitute an attractive future
644 therapy option for brain tumors when combined with multi-kinase inhibition.
645

bioRxiv preprint doi: https://doi.org/10.1101/2022.01.20.477108; this version posted January 22, 2022. The copyright holder for this preprint (which was not certified by peer review) is the author/funder, who has granted bioRxiv a license to display the preprint in perpetuity. It is made available under aCC-BY-NC-ND 4.0 International license.

Methods

Cell culture and reagents

Established human GB cell lines U87MG (gift from Ari Hinkkanen, University of Eastern Finland, Joensuu, Finland), A172, U118, U251 (gift from Pirjo Laakkonen, University of Helsinki, Helsinki, Finland), E98-FM-Cherry (gift from William Leenders, Radboud Institute for Molecular Life Sciences, Nijmegen, The Netherlands) and human fibroblasts (gift from Johanna Ivaska, Turku Bioscience, Turku, Finland) were cultured in DMEM (Sigma-Aldrich). T98G (VTT Technical Research Centre, Turku, Finland), DAOY (ATCC) and D283-Med (ATCC) were cultured in Eagle MEM (Sigma-Aldrich). All growth mediums were supplemented with 10% (except fibroblasts supplemented with 20%) of heat-inactivated fetal bovine serum (FBS) (Biowest), 2 mM L-glutamine and penicillin (50 U/mL)/ streptomycin (50 µg/mL). All cell cultures were maintained in a humified atmosphere of 5% CO_2 at 37°C.

The patient-derived GSCs BT3-CD133$^+$and BT12 (Kuopio University Hospital, Kuopio, Finland) (25,38) were cultured in DMEM/F12 (Gibco) and supplemented with 2 mM L-glutamine, 2% B27-supplement (Gibco), penicillin (50 U/mL) / streptomycin (50 µg/mL), 0.01 µg/mL hFGF-β (Peprotech), 0.02 µg/mL hEGF (Peprotech) and 15 mM HEPES-buffer (Gibco). For assays requiring adherent cell, such as colony growth, GSC populations were cultured on Matrigel (Becton Dickinson) coated plates.

The following chemicals were purchased from indicated distributors: AKT1/2 inhibitor, staurosporine, CEP-701, UCN-01, PKC412, sodium salt of dichloroacetate (DCA) and lipoic acid

bioRxiv preprint doi: https://doi.org/10.1101/2022.01.20.477108; this version posted January 22, 2022. The copyright holder for this preprint (which was not certified by peer review) is the author/funder, who has granted bioRxiv a license to display the preprint in perpetuity. It is made available under aCC-BY-NC-ND 4.0 International license.

669 from Sigma-Aldrich; FRAX486 and Vemurafenib from SelleckChem; K252a and rebeccamycin
670 from Enzo Life Sciences; K252c from Tocris Bioscience; MK-2206 from MedChemExpress.
671 Compound were dissolved in DMSO (Sigma-Aldrich) or mQ (for DCA) and stored at -20°C.
672 SMAPs (NZ-8-061, DBK-794, DBK-1154, DBK-1160 and DBK-766) were kindly supplied by Prof.
673 Michael Ohlmeyer (Icahn School of Medicine at the Mount Sinai, NY, USA), were dissolved in
674 DMSO and stored at room temperature protected from light.

675

676 **Cell viability assay**

677 Optimized numbers of cells (2.5 x 10^3 to 5 x 10^3) were plated onto 96-well plates (Perkin
678 Elmer) and allowed to adhere. After 24 hours, cells were treated with vehicle (DMSO) or the
679 indicated concentrations of compounds. After 72 hours, cell viability was measured using
680 CellTiter-Glo assay (Promega) according the manufacturer's instructions using a BioTek
681 Synergy H1 plate reader (BioTek).

682

683 **Colony formation assay**

684 Optimized numbers of cells (3 x 10^3 to 10 x 10^3) were seeded in either 12-well plates and
685 allowed to adhere. Matrigel matrix coated plates were used for patient-derived glioma stem
686 cells. After approximately 24 hours cells were treated with drugs. After 72 hours of
687 incubation, drug-containing media were replaced with non-drug containing medium and
688 incubated until the control wells were confluent. Cells were fixed with ice cold methanol and
689 stained with 0.2% crystal violet solution in 10% ethanol for 15 min at room temperature.
690 Plates were dried and scanned with Epson Perfection V700 Photo scanner. Quantification of

bioRxiv preprint doi: https://doi.org/10.1101/2022.01.20.477108; this version posted January 22, 2022. The copyright holder for this preprint (which was not certified by peer review) is the author/funder, who has granted bioRxiv a license to display the preprint in perpetuity. It is made available under aCC-BY-NC-ND 4.0 International license.

691 colonies were done with ImageJ by using the Colony area plugin (57). Data were normalized
692 and presented as a per cent of the control.
693
694 Colony formation assays at hypoxic conditions were performed in InvivO2 400 incubator
695 (Ruskinn Technology) at following conditions 1% O_2, 5% CO_2 and 90% humidity.
696
697 **Caspase-3 and -7 activity assay**
698 T98G cells (2.5 x 10^3) were plated in 96-well plates (Perkin Elmer) and allowed to adhere. After
699 24 hours, cells were treated with drugs for the next 24 hours. Pan-caspase inhibitor Z-VAD-
700 FMK (10 mM, Promega) was added at the same time as drugs. Caspase-3 and -7 activity was
701 measured by Caspase-Glo 3/7 Assay (Promega) according the manufacturer's instructions
702 using a BioTek Synergy H1 plate reader.
703
704 **Western blotting and antibodies**
705 Standard immunoblotting analysis was performed using the following primary antibodies:
706 AKT (Cell Signaling, 9272S, 1:1,000), phospho Akt S473 (Cell Signaling, 9271, 1:1,000), PME-1
707 (Santa Cruz, sc-20086, 1:1,000), β-actin (Sigma-Aldrich, A1978, 1:10,000), phospho PDHE1-A
708 type I (S300) (Millipore, ABS194, 1:1,000), cleaved PARP1 (E51) (Abcam, ab32064, 1:1,000)
709 and GAPDH (Hytest, 5G4cc, 1:10,000). Secondary antibodies were purchased from LI-COR,
710 mouse (926-32212) and rabbit (926-68021). The membranes were scanned using an Odyssey
711 scanner (Li-Cor Biosciences). Quantification of protein abundance was assessed with Image
712 Studio Lite (version 5.2) on three immunoblots from independent lysates.
713
714 **Chaperone binding assay**

bioRxiv preprint doi: https://doi.org/10.1101/2022.01.20.477108; this version posted January 22, 2022. The copyright holder for this preprint (which was not certified by peer review) is the author/funder, who has granted bioRxiv a license to display the preprint in perpetuity. It is made available under aCC-BY-NC-ND 4.0 International license.

715 LUMIER (LUminescence-based Mammalian IntERactome) with BACON (bait control) assay
716 was performed as previously described (35). In short, 3xFLAG-tagged bait proteins are
717 transfected into 293T cells expressing the Chaperone-Renilla (prey) luciferase in a 96-well
718 plate. After two days, cells are treated with kinase inhibitors (or DMSO) for 1 hour before cell
719 lysis. The cell lysates expressing each bait protein are applied to anti-FLAG coated 384-well
720 plates, which captures the bait protein. The amount of luminescence in the well, after
721 washing off nonspecifically binding proteins, indicates the interaction between the bait
722 protein with the prey protein. After the luminescence measurement, the amount of bait
723 protein is measured with ELISA, using a different, polyclonal anti-FLAG antibody conjugated
724 to horseradish peroxidase.
725
726 **Long-term growth assay**
727 E98 cells (3 x 10^3) were plated into 96-well plate. On the next day cells were treated with
728 DMSO, MK-2206 (7 µM), DCA (20 mM), NZ-8-061 (10 µM) alone, or in their double or triplet
729 combinations (6-12 wells/condition). Every 3-4 days medium was replaced with fresh media
730 with or without drugs. The confluency of the wells was determined daily using IncuCyte ZOOM
731 live cell analysis system (Essen Bioscience).
732
733 **Mitochondrial respiration measurement**
734 Agilent Seahorse XF Cell Mito Stress Test (Agilent Seahorse Bioscience) was applied to T98G
735 cells according the manufacturer's instructions. In short, T98G cells were seeded at 1 x 10^4
736 cells per well in a Seahorse 96-well XF Cell Culture microplate in 100 µL of the growing
737 medium. On the next day cells were treated with DMSO, DCA (10 mM), MK-2206 (7 µM) alone
738 or in combination with NZ-8-061 (10 µM) for the next 24 hours. On the day of analysis, the

bioRxiv preprint doi: https://doi.org/10.1101/2022.01.20.477108; this version posted January 22, 2022. The copyright holder for this preprint (which was not certified by peer review) is the author/funder, who has granted bioRxiv a license to display the preprint in perpetuity. It is made available under aCC-BY-NC-ND 4.0 International license.

739 growth media were replaced with 120 µL of XF assay media (non-buffered DMEM
740 supplemented with 10 mM glucose, 1 mM sodium pyruvate and 2 mM glutamine) and
741 incubated at 37°C in a non-CO_2 incubator for one hour before running assay. Mitochondrial
742 function of the cells was analyzed by sequential injections of modulators, oligomycin,
743 carbonyl cyanide-4 (trifluoromethoxy) phenylhydrazone (FCCP), and rotenone/antimycin A,
744 at Seahorse XFe96 analyzer (Agilent Seahorse Bioscience). The Seahorse XF Mito Stress Test
745 Report Generator was used to calculate the Seahorse XF Cell Mito Stress Test parameters
746 from Wave software (version 2.6.153). The data were normalized to total protein per well
747 using BCA assay (Thermo Fisher Scientific).
748
749 **BH3 profiling**
750 BH3 profiling was performed as previously described (46,47). In brief, T98G cells were
751 pretreated with DMSO, MK-2206 (5 µM), DCA (20 mM), NZ-8-061 (8 µM) alone, or in their
752 double or triplet combinations for 24 hours. On the next day, cells were permeabilized with
753 0.002% digitonin and treated with a library of synthetic peptides. Peptides used were BIM at
754 0.01 µM, BAD, HRK and MS1 at 10 µM. The BIM peptide assesses the functionality of BAX and
755 BAK. BAD binds and antagonizes BCL-2, BCL-xL, BCL-W, and BFL-1. HRK specifically binds and
756 antagonizes BCL-xL. MS1 binds and antagonizes MCL-1. A pore-forming peptide, alamethicin
757 (positive control), or DMSO (negative control) served as controls. Cells were incubated with
758 the peptides for half an hour at 25°C and subsequently fixed with 4% paraformaldehyde for
759 10 min. Finally, intracellular cytochrome *c* was stained with an immunofluorescence-labeled
760 antibody (BioLegend Alexa Fluor 647 anti-Cytochrome *c* Antibody, clone 6H2.B4). Relative
761 cytochrome *c* release was assessed by formula 1 – [(sample-pos.ctrl.)/(neg.ctrl.-pos.ctrl.)].
762

bioRxiv preprint doi: https://doi.org/10.1101/2022.01.20.477108; this version posted January 22, 2022. The copyright holder for this preprint (which was not certified by peer review) is the author/funder, who has granted bioRxiv a license to display the preprint in perpetuity. It is made available under aCC-BY-NC-ND 4.0 International license.

763 **Bioinformatics analysis**

764 Cytoscape network analysis software (version 3.9.0) (58) was used to visualize the STRING
765 interactive map of hit kinases (59). For calculation and visualization of synergy scores, dose-
766 response matrix of NZ-8-061 and UCN-01 combination data were applied to SynergyFinder
767 (version 2.0) web-application (60).

768

769 **Statistical analyses**

770 For cell culture experiments, three biological replicates have been performed, and each
771 condition was tested in triplicate, unless otherwise specified. Data are presented as mean ±
772 SD and statistical analyses were carried out using a two-tailed Student's t-test assuming
773 unequal variances. For *in vivo* experiments, the following statistical tests were chosen
774 depending on the results of the preliminary Shapiro-Wilk test of data normality. Two way
775 ANOVA with Tukey's multiple comparisons test were used to assess differences between
776 three or more experimental groups. Lonk-rank (Mantel-Cox) test was used in survival analysis.
777 These univariate statistical analyses were performed using GraphPad Prism 9 software
778 (GraphPad Software). $P < 0.05$ was considered statistically significant.

779

780 **Supplementary Materials**

781 Supplementary Methods and Figures S1-7.

782 Table S1. Chaperone interaction assay data.

783 Table S2. 28 kinase hit list.

784 Table S3. The customer kinase siRNA library.

785 Table S4. Inhibitor selectivity data.

bioRxiv preprint doi: https://doi.org/10.1101/2022.01.20.477108; this version posted January 22, 2022. The copyright holder for this preprint (which was not certified by peer review) is the author/funder, who has granted bioRxiv a license to display the preprint in perpetuity. It is made available under aCC-BY-NC-ND 4.0 International license.

Table S5. Significantly ($p < 0.05$) regulated phosphopeptides from triplet therapy treated DAOY xenografts.

Table S6. Enriched Reactome pathways based on Table S5.

Table S7. The list of the used siRNA.

Competing interests

Authors declare no competing interests.

Authors' Contributions

Conception and design: O.V.D., J.M., A.K. J.W. Development of methodology: O.V.D., J.M., R.H., X.Q., J.W. Experimental work: M.T., O.V.D., C.S-F., K.W. R.K., M.P., O.K. Bioinformatic analysis: M.J., L.Y., O.K., T.A. In vivo work: O.V.D., J.M., R.H. Resources: M.O. Writing: O.V.D., J.M., T.A., J.W.

Acknowledgements

Authors want to acknowledge Turku Center for Disease Modelling (TCDM) and Made Consulting for expert help with mouse experiments, Artur Padzic for help and expertise with lentivirus experiments, William Eccleshall and Mung Kwan Long for help with Seahorse experiments, and Kari Kurppa for expert help with Incucyte experiments and for helpful discussions. Johanna Ivaska is thanked for comments on the manuscript. Taina Kalevo-Mattila is acknowledged for excellent technical support as well as the entire Turku Bioscience personnel for excellent working environment.

bioRxiv preprint doi: https://doi.org/10.1101/2022.01.20.477108; this version posted January 22, 2022. The copyright holder for this preprint (which was not certified by peer review) is the author/funder, who has granted bioRxiv a license to display the preprint in perpetuity. It is made available under aCC-BY-NC-ND 4.0 International license.

Funding

Project was funded by Jane and Aatos Erkko Foundation, Finnish Cultural Foundation, Sigrid Juselius Foundation, K.Albin Johanssons Foundation, AAMU Suomen Lasten Syöpäsäätiö, Turku Doctoral Programme of Molecular Medicine, Academy of Finland, and Finnish Cancer Foundation.

bioRxiv preprint doi: https://doi.org/10.1101/2022.01.20.477108; this version posted January 22, 2022. The copyright holder for this preprint (which was not certified by peer review) is the author/funder, who has granted bioRxiv a license to display the preprint in perpetuity. It is made available under aCC-BY-NC-ND 4.0 International license.

References

1. Cohen P, Cross D, Janne PA. Kinase drug discovery 20 years after imatinib: progress and future directions. Nat Rev Drug Discov **2021**;20(7):551-69 doi 10.1038/s41573-021-00195-4.

2. Attwood MM, Fabbro D, Sokolov AV, Knapp S, Schioth HB. Trends in kinase drug discovery: targets, indications and inhibitor design. Nat Rev Drug Discov **2021**;20(11):839-61 doi 10.1038/s41573-021-00252-y.

3. Brennan CW, Verhaak RG, McKenna A, Campos B, Noushmehr H, Salama SR*, et al.* The somatic genomic landscape of glioblastoma. Cell **2013**;155(2):462-77 doi 10.1016/j.cell.2013.09.034.

4. Cruz Da Silva E, Mercier MC, Etienne-Selloum N, Dontenwill M, Choulier L. A Systematic Review of Glioblastoma-Targeted Therapies in Phases II, III, IV Clinical Trials. Cancers (Basel) **2021**;13(8) doi 10.3390/cancers13081795.

5. Dunn GP, Rinne ML, Wykosky J, Genovese G, Quayle SN, Dunn IF*, et al.* Emerging insights into the molecular and cellular basis of glioblastoma. Genes Dev **2012**;26(8):756-84 doi 10.1101/gad.187922.112.

6. Shen S, Vagner S, Robert C. Persistent Cancer Cells: The Deadly Survivors. Cell **2020**;183(4):860-74 doi 10.1016/j.cell.2020.10.027.

7. Konieczkowski DJ, Johannessen CM, Garraway LA. A Convergence-Based Framework for Cancer Drug Resistance. Cancer Cell **2018**;33(5):801-15 doi 10.1016/j.ccell.2018.03.025.

bioRxiv preprint doi: https://doi.org/10.1101/2022.01.20.477108; this version posted January 22, 2022. The copyright holder for this preprint (which was not certified by peer review) is the author/funder, who has granted bioRxiv a license to display the preprint in perpetuity. It is made available under aCC-BY-NC-ND 4.0 International license.

8. Smith MP, Wellbrock C. Molecular Pathways: Maintaining MAPK Inhibitor Sensitivity by Targeting Nonmutational Tolerance. Clin Cancer Res **2016**;22(24):5966-70 doi 10.1158/1078-0432.CCR-16-0954.

9. Westermarck J. Targeted therapies don't work for a reason; the neglected tumor suppressor phosphatase PP2A strikes back. FEBS J **2018**;285(22):4139-45 doi 10.1111/febs.14617.

10. Klaeger S, Heinzlmeir S, Wilhelm M, Polzer H, Vick B, Koenig PA*, et al.* The target landscape of clinical kinase drugs. Science **2017**;358(6367) doi 10.1126/science.aan4368.

11. Lin A, Giuliano CJ, Palladino A, John KM, Abramowicz C, Yuan ML*, et al.* Off-target toxicity is a common mechanism of action of cancer drugs undergoing clinical trials. Science translational medicine **2019**;11(509) doi 10.1126/scitranslmed.aaw8412.

12. Montoya S, Soong D, Nguyen N, Affer M, Munamarty SP, Taylor J. Targeted Therapies in Cancer: To Be or Not to Be, Selective. Biomedicines **2021**;9(11) doi 10.3390/biomedicines9111591.

13. Gani OA, Engh RA. Protein kinase inhibition of clinically important staurosporine analogues. Natural product reports **2010**;27(4):489-98 doi 10.1039/b923848b.

14. Tang J, Tanoli ZUR, Ravikumar B, Alam Z, Rebane A, Vaha-Koskela M*, et al.* Drug Target Commons: A Community Effort to Build a Consensus Knowledge Base for Drug-Target Interactions. Cell Chem Biol **2018**;25(2):224-+ doi 10.1016/j.chembiol.2017.11.009.

15. Gimple RC, Bhargava S, Dixit D, Rich JN. Glioblastoma stem cells: lessons from the tumor hierarchy in a lethal cancer. Genes Dev **2019**;33(11-12):591-609 doi 10.1101/gad.324301.119.

bioRxiv preprint doi: https://doi.org/10.1101/2022.01.20.477108; this version posted January 22, 2022. The copyright holder for this preprint (which was not certified by peer review) is the author/funder, who has granted bioRxiv a license to display the preprint in perpetuity. It is made available under aCC-BY-NC-ND 4.0 International license.

16. Patel AP, Tirosh I, Trombetta JJ, Shalek AK, Gillespie SM, Wakimoto H*, et al.* Single-cell RNA-seq highlights intratumoral heterogeneity in primary glioblastoma. Science **2014**;344(6190):1396-401 doi 10.1126/science.1254257.

17. Hoxhaj G, Manning BD. The PI3K-AKT network at the interface of oncogenic signalling and cancer metabolism. Nature Reviews Cancer **2020**;20(2):74-88 doi 10.1038/s41568-019-0216-7.

18. Agnihotri S, Zadeh G. Metabolic reprogramming in glioblastoma: the influence of cancer metabolism on epigenetics and unanswered questions. Neuro-oncology **2016**;18(2):160-72 doi 10.1093/neuonc/nov125.

19. Michelakis ED, Sutendra G, Dromparis P, Webster L, Haromy A, Niven E*, et al.* Metabolic modulation of glioblastoma with dichloroacetate. Science translational medicine **2010**;2(31):31ra4 doi 10.1126/scitranslmed.3000677.

20. Wang Z, Peet NP, Zhang P, Jiang Y, Rong L. Current Development of Glioblastoma Therapeutic Agents. Molecular cancer therapeutics **2021**;20(9):1521-32 doi 10.1158/1535-7163.MCT-21-0159.

21. Alexandru O, Horescu C, Sevastre AS, Cioc CE, Baloi C, Oprita A*, et al.* Receptor tyrosine kinase targeting in glioblastoma: performance, limitations and future approaches. Contemp Oncol (Pozn) **2020**;24(1):55-66 doi 10.5114/wo.2020.94726.

22. Kauko O, Westermarck J. Non-genomic mechanisms of protein phosphatase 2A (PP2A) regulation in cancer. Int J Biochem Cell Biol **2018**;96:157-64 doi 10.1016/j.biocel.2018.01.005.

23. Fowle H, Zhao Z, Grana X. PP2A holoenzymes, substrate specificity driving cellular functions and deregulation in cancer. Adv Cancer Res **2019**;144:55-93 doi 10.1016/bs.acr.2019.03.009.

bioRxiv preprint doi: https://doi.org/10.1101/2022.01.20.477108; this version posted January 22, 2022. The copyright holder for this preprint (which was not certified by peer review) is the author/funder, who has granted bioRxiv a license to display the preprint in perpetuity. It is made available under aCC-BY-NC-ND 4.0 International license.

883 24. Kauko O, O'Connor CM, Kulesskiy E, Sangodkar J, Aakula A, Izadmehr S*, et al.* PP2A
884 inhibition is a druggable MEK inhibitor resistance mechanism in KRAS-mutant lung
885 cancer cells. Science translational medicine **2018**;10(450) doi
886 10.1126/scitranslmed.aaq1093.
887 25. Merisaari J, Denisova OV, Doroszko M, Le Joncour V, Johansson P, Leenders WPJ*, et*
888 *al.* Monotherapy efficacy of blood-brain barrier permeable small molecule
889 reactivators of protein phosphatase 2A in glioblastoma. Brain Communications
890 **2020**;2(1) doi ARTN 02 10.1093/braincomms/fcaa002.
891 26. Qin S, Li J, Si Y, He Z, Zhang T, Wang D*, et al.* Cucurbitacin B induces inhibitory effects
892 via CIP2A/PP2A/Akt pathway in glioblastoma multiforme. Mol Carcinog
893 **2018**;57(6):687-99 doi 10.1002/mc.22789.
894 27. Puustinen P, Junttila MR, Vanhatupa S, Sablina AA, Hector ME, Teittinen K*, et al.* PME-
895 1 Protects Extracellular Signal-Regulated Kinase Pathway Activity from Protein
896 Phosphatase 2A-Mediated Inactivation in Human Malignant Glioma. Cancer Research
897 **2009**;69(7):2870-7 doi 10.1158/0008-5472.Can-08-2760.
898 28. Kaur A, Denisova OV, Qiao X, Jumppanen M, Peuhu E, Ahmed SU*, et al.* PP2A Inhibitor
899 PME-1 Drives Kinase Inhibitor Resistance in Glioma Cells. Cancer Research
900 **2016**;76(23):7001-11 doi 10.1158/0008-5472.Can-16-1134.
901 29. Vainonen JP, Momeny M, Westermarck J. Druggable cancer phosphatases. Science
902 translational medicine **2021**;13(588) doi 10.1126/scitranslmed.abe2967.
903 30. Akimov Y, Aittokallio T. Re-defining synthetic lethality by phenotypic profiling for
904 precision oncology. Cell Chem Biol **2021**;28(3):246-56 doi
905 10.1016/j.chembiol.2021.01.026.

bioRxiv preprint doi: https://doi.org/10.1101/2022.01.20.477108; this version posted January 22, 2022. The copyright holder for this preprint (which was not certified by peer review) is the author/funder, who has granted bioRxiv a license to display the preprint in perpetuity. It is made available under aCC-BY-NC-ND 4.0 International license.

906 31. Kaur A, Westermarck J. Regulation of protein phosphatase 2A (PP2A) tumor
907 suppressor function by PME-1. Biochem Soc Trans **2016**;44(6):1683-93 doi
908 10.1042/BST20160161.
909 32. Sangodkar J, Perl A, Tohme R, Kiselar J, Kastrinsky DB, Zaware N*, et al.* Activation of
910 tumor suppressor protein PP2A inhibits KRAS-driven tumor growth. J Clin Invest
911 **2017**;127(6):2081-90 doi 10.1172/JCI89548.
912 33. Vit G, Duro J, Rajendraprasad G, Hertz EPT, Kauffeldt Holland LK, Weisser MB*, et al.*
913 Cellular toxicity of iHAP1 and DT-061 does not occur through PP2A-B56 targeting.
914 bioRxiv **2021**:2021.07.08.451586 doi 10.1101/2021.07.08.451586.
915 34. Taipale M. Quantitative Profiling of Chaperone/Client Interactions with LUMIER Assay.
916 Methods Mol Biol **2018**;1709:47-58 doi 10.1007/978-1-4939-7477-1_4.
917 35. Taipale M, Krykbaeva I, Whitesell L, Santagata S, Zhang J, Liu Q*, et al.* Chaperones as
918 thermodynamic sensors of drug-target interactions reveal kinase inhibitor specificities
919 in living cells. Nature biotechnology **2013**;31(7):630-7 doi 10.1038/nbt.2620.
920 36. Shariati M, Meric-Bernstam F. Targeting AKT for cancer therapy. Expert Opin Investig
921 Drugs **2019**;28(11):977-88 doi 10.1080/13543784.2019.1676726.
922 37. Stacpoole PW. Therapeutic Targeting of the Pyruvate Dehydrogenase
923 Complex/Pyruvate Dehydrogenase Kinase (PDC/PDK) Axis in Cancer. Journal of the
924 National Cancer Institute **2017**;109(11) doi 10.1093/jnci/djx071.
925 38. Le Joncour V, Filppu P, Hyvonen M, Holopainen M, Turunen SP, Sihto H*, et al.*
926 Vulnerability of invasive glioblastoma cells to lysosomal membrane destabilization.
927 EMBO Mol Med **2019**;11(6) doi 10.15252/emmm.201809034.

bioRxiv preprint doi: https://doi.org/10.1101/2022.01.20.477108; this version posted January 22, 2022. The copyright holder for this preprint (which was not certified by peer review) is the author/funder, who has granted bioRxiv a license to display the preprint in perpetuity. It is made available under aCC-BY-NC-ND 4.0 International license.

928 39. Mooney J, Bernstock JD, Ilyas A, Ibrahim A, Yamashita D, Markert JM*, et al.* Current
929 Approaches and Challenges in the Molecular Therapeutic Targeting of Glioblastoma.
930 World Neurosurg **2019**;129:90-100 doi 10.1016/j.wneu.2019.05.205.
931 40. Wen J, Hadden MK. Medulloblastoma drugs in development: Current leads, trials and
932 drawbacks. Eur J Med Chem **2021**;215:113268 doi 10.1016/j.ejmech.2021.113268.
933 41. Di Magno L, Manzi D, D'Amico D, Coni S, Macone A, Infante P*, et al.* Druggable
934 glycolytic requirement for Hedgehog-dependent neuronal and medulloblastoma
935 growth. Cell Cycle **2014**;13(21):3404-13 doi 10.4161/15384101.2014.952973.
936 42. Austin JA, Jenkins RE, Austin GM, Glenn MA, Dunn K, Scott L*, et al.* Cancerous inhibitor
937 of protein phosphatase 2A (CIP2A) modifies energy metabolism via 5' AMP-activated
938 protein kinase signalling in malignant cells. Biochem J **2019**;476(15):2255-69 doi
939 10.1042/BCJ20190121.
940 43. Atas E, Oberhuber M, Kenner L. The Implications of PDK1-4 on Tumor Energy
941 Metabolism, Aggressiveness and Therapy Resistance. Frontiers in oncology
942 **2020**;10:583217 doi 10.3389/fonc.2020.583217.
943 44. Bosc C, Saland E, Bousard A, Gadaud G, Sabatier M, Cognet G*, et al.* Mitochondrial
944 inhibitors circumvent adaptive resistance to venetoclax and cytarabine combination
945 therapy in acute myeloid leukemia. Nature Cancer **2021**;2:1204–23.
946 45. Potter DS, Letai A. To Prime, or Not to Prime: That Is the Question. Cold Spring Harbor
947 symposia on quantitative biology **2016**;81:131-40 doi 10.1101/sqb.2016.81.030841.
948 46. Koch R, Christie AL, Crombie JL, Palmer AC, Plana D, Shigemori K*, et al.* Biomarker-
949 driven strategy for MCL1 inhibition in T-cell lymphomas. Blood **2019**;133(6):566-75 doi
950 10.1182/blood-2018-07-865527.

bioRxiv preprint doi: https://doi.org/10.1101/2022.01.20.477108; this version posted January 22, 2022. The copyright holder for this preprint (which was not certified by peer review) is the author/funder, who has granted bioRxiv a license to display the preprint in perpetuity. It is made available under aCC-BY-NC-ND 4.0 International license.

951 47. Ryan J, Montero J, Rocco J, Letai A. iBH3: simple, fixable BH3 profiling to determine
952 apoptotic priming in primary tissue by flow cytometry. Biol Chem **2016**;397(7):671-8
953 doi 10.1515/hsz-2016-0107.
954 48. Xie Q, Wu Q, Kim L, Miller TE, Liau BB, Mack SC*, et al.* RBPJ maintains brain tumor-
955 initiating cells through CDK9-mediated transcriptional elongation. J Clin Invest
956 **2016**;126(7):2757-72 doi 10.1172/JCI86114.
957 49. Vervoort SJ, Welsh SA, Devlin JR, Barbieri E, Knight DA, Offley S*, et al.* The PP2A-
958 Integrator-CDK9 axis fine-tunes transcription and can be targeted therapeutically in
959 cancer. Cell **2021**;184(12):3143-62 e32 doi 10.1016/j.cell.2021.04.022.
960 50. Dhanasekaran DN, Reddy EP. JNK signaling in apoptosis. Oncogene **2008**;27(48):6245-
961 51 doi 10.1038/onc.2008.301.
962 51. Kaley TJ, Panageas KS, Mellinghoff IK, Nolan C, Gavrilovic IT, DeAngelis LM*, et al.* Phase
963 II trial of an AKT inhibitor (perifosine) for recurrent glioblastoma. J Neurooncol
964 **2019**;144(2):403-7 doi 10.1007/s11060-019-03243-7.
965 52. Wen PY, Touat M, Alexander BM, Mellinghoff IK, Ramkissoon S, McCluskey CS*, et al.*
966 Buparlisib in Patients With Recurrent Glioblastoma Harboring Phosphatidylinositol 3-
967 Kinase Pathway Activation: An Open-Label, Multicenter, Multi-Arm, Phase II Trial. J
968 Clin Oncol **2019**;37(9):741-50 doi 10.1200/JCO.18.01207.
969 53. Dunbar EM, Coats BS, Shroads AL, Langaee T, Lew A, Forder JR*, et al.* Phase 1 trial of
970 dichloroacetate (DCA) in adults with recurrent malignant brain tumors. Investigational
971 new drugs **2014**;32(3):452-64 doi 10.1007/s10637-013-0047-4.
972 54. Oshima N, Ishida R, Kishimoto S, Beebe K, Brender JR, Yamamoto K*, et al.* Dynamic
973 Imaging of LDH Inhibition in Tumors Reveals Rapid In Vivo Metabolic Rewiring and

bioRxiv preprint doi: https://doi.org/10.1101/2022.01.20.477108; this version posted January 22, 2022. The copyright holder for this preprint (which was not certified by peer review) is the author/funder, who has granted bioRxiv a license to display the preprint in perpetuity. It is made available under aCC-BY-NC-ND 4.0 International license.

974 Vulnerability to Combination Therapy. Cell reports **2020**;30(6):1798-810 e4 doi
975 10.1016/j.celrep.2020.01.039.
976 55. Ly JD, Grubb DR, Lawen A. The mitochondrial membrane potential (deltapsi(m)) in
977 apoptosis; an update. Apoptosis **2003**;8(2):115-28 doi 10.1023/a:1022945107762.
978 56. Garner EF, Williams AP, Stafman LL, Aye JM, Mroczek-Musulman E, Moore BP*, et al.*
979 FTY720 Decreases Tumorigenesis in Group 3 Medulloblastoma Patient-Derived
980 Xenografts. Scientific reports **2018**;8(1):6913 doi 10.1038/s41598-018-25263-5.
981 57. Guzman C, Bagga M, Kaur A, Westermarck J, Abankwa D. ColonyArea: an ImageJ plugin
982 to automatically quantify colony formation in clonogenic assays. PloS one
983 **2014**;9(3):e92444 doi 10.1371/journal.pone.0092444.
984 58. Shannon P, Markiel A, Ozier O, Baliga NS, Wang JT, Ramage D*, et al.* Cytoscape: a
985 software environment for integrated models of biomolecular interaction networks.
986 Genome research **2003**;13(11):2498-504.
987 59. Szklarczyk D, Gable AL, Nastou KC, Lyon D, Kirsch R, Pyysalo S*, et al.* The STRING
988 database in 2021: customizable protein-protein networks, and functional
989 characterization of user-uploaded gene/measurement sets. Nucleic Acids Res
990 **2021**;49(D1):D605-D12 doi 10.1093/nar/gkaa1074.
991 60. Ianevski A, Giri AK, Aittokallio T. SynergyFinder 2.0: visual analytics of multi-drug
992 combination synergies. Nucleic Acids Res **2020**;48(W1):W488-W93 doi
993 10.1093/nar/gkaa216.
994